

Fast Learnings of Coupled Nonnegative Tensor Decomposition Using Optimal Gradient and Low-rank Approximation

Xiulin Wang, Jing Liu and Fengyu Cong

Abstract—Tensor decomposition is a fundamental technique widely applied in signal processing, machine learning, and various other fields. However, traditional tensor decomposition methods encounter limitations when jointly analyzing multi-block tensors, as they often struggle to effectively explore shared information among tensors. In this study, we first introduce a novel coupled nonnegative CANDECOMP/PARAFAC decomposition algorithm optimized by the alternating proximal gradient method (CoNCPD-APG). This algorithm is specially designed to address the challenges of jointly decomposing different tensors that are partially or fully linked, while simultaneously extracting common components, individual components and, core tensors. Recognizing the computational challenges inherent in optimizing nonnegative constraints over high-dimensional tensor data, we further propose the IraCoNCPD-APG algorithm. By integrating low-rank approximation with the proposed CoNCPD-APG method, the proposed algorithm can significantly decrease the computational burden without compromising decomposition quality, particularly for multi-block large-scale tensors. Simulation experiments conducted on synthetic data, real-world face image data, and two kinds of electroencephalography (EEG) data demonstrate the practicality and superiority of the proposed algorithms for coupled nonnegative tensor decomposition problems. Our results underscore the efficacy of our methods in uncovering meaningful patterns and structures from complex multi-block tensor data, thereby offering valuable insights for future applications.

Index Terms—Alternating proximal gradient, CANDECOMP/PARAFAC, coupled tensor decomposition, low-rank approximation, nonnegative tensor decomposition

I. INTRODUCTION

DECOMPOSING a tensor into a minimal number of rank-1 tensors is known as CANDECOMP/PARAFAC (or Canonical Polyadic, [1, 2, 3]) decomposition (CPD). Nonnegative CPD (NCPD) imposes nonnegative constraints on its latent factors, providing a part-based representation of a tensor that can extract more meaningful and convincing information [4]. For instance, electroencephalography (EEG) data, characterized by spatial, temporal, and subject dimensions,

can be represented as a third-order tensor, with underlying features extractable through CPD [5]. When considering the time-frequency representation, non-negativity will be naturally brought into the EEG data, making NCPD a necessary method[6]. CPD and NCPD methods have garnered significant attention in both theory and application, primarily focusing on the analysis of tensors from a single dataset [7, 8, 9]. When it comes to emerging multi-block tensors, such as multi-subject or multi-modal biomedical data that require joint analysis, traditional tensor decomposition methods become quite challenging in effectively identifying the interconnections among different tensors [10, 11]. For example, traditional methods are inadequate for resolving the internal sharing within EEG data from multiple subjects, or integrating the complementary spatiotemporal characteristics in EEG-fMRI data [11, 12].

Coupled tensor decomposition, an extension of tensor decomposition to multi-block tensors, allows for the simultaneous decomposition of two or more tensors with an enforced shared structure [10, 13, 14]. Notably, the uniqueness condition for coupled tensor decomposition is more relaxed compared to that of single tensor decomposition [14, 15]. This method can leverage various constraints, such as sparsity, smoothness, and nonnegativity, to obtain more unique solutions and interpretable components [16, 17]. By preserving the multi-way structure of tensor data, Coupled tensor decomposition can achieve higher decomposition accuracy and robustness, revealing interconnections among tensor data that would inevitably be lost in two-way matrix counterparts [5, 11, 16, 18, 19], while coupled tensor methods can circumvent the independent constraint [15, 20]. Moreover, coupled tensor decomposition of multi-block tensors can achieve the simultaneous extraction of common components shared by all tensors and individual components specific to each tensor [21, 22, 23].

To date, increasing recognition of joint tensor analysis has spurred the exploration of coupled tensor decomposition in various applications. In certain cases, coupled matrix and tensor factorization (CMTF [24]) and its derivatives [12, 25, 26, 27], such as advanced CMTF [25] and coupled tensor-tensor decomposition (CTTD [12, 26]), have demonstrated their superiority over ICA-based two-way methods in fusing EEG and fMRI data. The algebraic double-coupled CPD (DC-CPD) algorithm, which uses second-order statistics in joint blind source separation problems, exhibits greater uniqueness and accuracy than the standard CPD [13]. Linked CPD models, optimized by hierarchical alternating least squares (HALS),

Corresponding authors: Jing Liu, email: liujing@dmu.edu.cn; Fengyu Cong, email: cong@dlut.edu.cn

X. Wang and J. Liu are with the Stem Cell Clinical Research Center, The First Affiliated Hospital of Dalian Medical University, Dalian 116011, China and also Dalian Innovation Institute of Stem Cell and Precision Medicine, Dalian 116085, China. X. Wang and F. Cong are with the Faculty of Information Technology, University of Jyväskylä, Jyväskylä 40100, Finland. F. Cong is also with School of Biomedical Engineering, Faculty of Medicine, Dalian University of Technology, Dalian, China and Key Laboratory of Social Computing and Cognitive Intelligence (Dalian University of Technology), Ministry of Education, China. Xiulin Wang: xiulin.wang@foxmail.com

Manuscript received Month Day, Year; revised Month Day, Year.

fast HALS, and alternating direction method of multipliers (ADMM), have also achieved good performance in classification, image processing, and biomedical signal processing [11, 21, 28, 29]. Additionally, the common and individual feature extraction (CIFE, [23]) framework for multi-block data facilitates the separate extraction of common and individual components by incorporating dimension reduction and blind source separation (BSS) methods, and has been successfully applied to classification, clustering and linked BSS problems [10]. Coupled tensor decomposition also finds applications in data fusion of low spatial resolution hyperspectral (LRHS) and high spatial resolution multispectral (HRMS) images [30, 31, 32], array signal processing [33, 34, 35], linked prediction[36] and metabolic physiology [37].

Nevertheless, existing coupled tensor decomposition methods often face challenges such as slow convergence speed and low optimization accuracy, primarily arising from the non-negative constraint and the high-dimensional nature of tensor data [38, 39]. Therefore, aiming to address these challenges and achieve effective and efficient joint tensor analysis with coupled information, we propose two advanced coupled NCPD methods: the coupled nonnegative CANDECOMP/PARAFAC decomposition algorithm based on alternating proximal gradient (CoNCPD-APG) and its fast implementation incorporating low-rank approximation (IraCoNCPD-APG). Specifically, our contributions in this study are outlined as follows:

- 1) Using the optimal gradient method, we propose an effective CoNCPD-APG algorithm for joint analysis of partially or fully linked multi-block tensors, which enables simultaneous decomposition of tensors with excellent decomposition accuracy.
- 2) By introducing low-rank approximation, we further propose an efficient larCoNCPD-APG algorithm, which can greatly reduce time consumption without losing decomposition accuracy.
- 3) We thoroughly analyze the types of couplings, algorithmic error bound and computational complexity, while also providing an insight into calculating the number of coupled tensor components.
- 4) The experiments designed on synthetic data, real-world face image and two types of EEG data prove the practicability and superiority of the proposed algorithms.

The rest of this paper is organized as follows. Section II introduces some basic preliminaries and related work. In Section III, we present the proposed algorithms as well as some theoretical analyses. Experiments on synthetic and real-world data are performed in Section IV to verify the performance of the proposed algorithms. The last section concludes this paper.

II. PRELIMINARIES AND RELATED WORK

A. Notations and tensor operations

Tensor, also known as multi-way array, is the high-order generalization of vector and matrix. The order of a tensor is the number of dimensions, ways or modes of itself. In this study, tensors are represented by calligraphic boldface uppercase letters, matrices by boldface uppercase letters, vectors by boldface uppercase letters, and scalars by lowercase letters.

Table I gives a summary of basic notations and mathematical operations throughout this study, and please refer to [7] for a more detailed description of them.

TABLE I
BASIC NOTATIONS AND MATHEMATICAL OPERATIONS

Symbol	Definition
\mathbb{R}, \mathbb{R}_+	real number, nonnegative real number
\circ, \odot	outer product, Khatri-Rao product
\otimes, \oslash	element-wise (Hadamard) product, division
$(\cdot)^T, \text{vec}(\cdot)$	transpose, vectorization operator
$\llbracket \cdot \rrbracket, \langle \cdot, \cdot \rangle, \ \cdot\ _F$	Kruskal operator, inner product and Frobenius norm
$m, \mathbf{m}, \mathbf{M}, \mathcal{M}$	scalar, vector, matrix and tensor
$\mathcal{M}_{(n)}$	mode- n matricization of tensor \mathcal{M}
$\text{vec}(\mathcal{M})$	vectorization of tensor \mathcal{M}
$\text{ddiag}(\mathcal{M})$	vectorization of super-diagonal elements of tensor \mathcal{M}
$\text{ddiag}(\mathbf{m})$	tensorization with \mathbf{m} on the super-diagonal elements
$U_{i:j,:}$	row-wise submatrix of U , i th to j th row
$U_{:,i:j}$	column-wise submatrix of U , i th to j th column
$U^{(n)}$	the n -th factor matrix
U^\odot	$U^{(N)} \odot U^{(N-1)} \odot \dots \odot U^{(2)} \dots \odot U^{(1)}$
$U^{\odot-n}$	$U^{(N)} \odot \dots \odot U^{(n+1)} \odot U^{(n-1)} \dots \odot U^{(1)}$
U^\otimes	$U^{(N)} \otimes U^{(N-1)} \otimes \dots \otimes U^{(2)} \dots \otimes U^{(1)}$
$U^{\otimes-n}$	$U^{(N)} \otimes \dots \otimes U^{(n+1)} \otimes U^{(n-1)} \dots \otimes U^{(1)}$

B. Optimal gradient method

Accelerated/Alternating proximal gradient (APG), an accelerated version of proximal gradient (PG, [40]), was originally proposed by Nesterov for smooth optimization with achieving the convergence rate of $\mathcal{O}(\frac{1}{K^2})$, where K is the number of iterations [41, 42]. For a minimization problem: $\min\{f(x), x \in \mathbb{R}^n\}$, assuming that $f(x) : \mathbb{R}^n \rightarrow \mathbb{R}$ is a convex function with Lipschitz continuous gradient f' , there will hold that

$$\|f'(x_i) - f'(x_j)\| \leq L \|x_i - x_j\|, \forall x_i, x_j \in \mathbb{R}^n, \quad (1)$$

where $L > 0$ is the Lipschitz constant. To obtain an optimal point \ddot{x} , two sequences are updated successively in each iteration round (assume at the k th iteration) in APG method [41, 43] as follows:

$$x_k = \underset{x}{\text{argmin}} \left\{ \phi(x, x_{k-1}) = f(x_{k-1}) + \langle x - x_{k-1}, f'(x_{k-1}) \rangle + \frac{L}{2} \|x - x_{k-1}\|^2 \right\}, \quad (2)$$

and

$$x_{k+1} = x_k + \frac{\alpha_k - 1}{\alpha_{k+1}} (x_k - x_{k-1}) \quad (3)$$

with

$$\alpha_0 = 1, \alpha_{k+1} = \frac{1 + \sqrt{4\alpha_k^2 + 1}}{2} \quad (4)$$

where $\phi(x, x_{k-1})$ denotes the proximal regularized function of $f(x)$ at x_{k-1} and (3) denotes an extrapolated point by combining the points of current and previous iterations. Using the Lagrange multiplier method, from (2), we have

$$x_k \leftarrow \mathcal{P}(x_{k-1} - \frac{1}{L} f'(x_{k-1})) \quad (5)$$

where $\mathcal{P}(\cdot)$ denotes a shrinkage operator predefined by the user. Since each subproblem under block coordinate descent (BCD) framework is a convex function with Lipschitz continuous gradient, APG and its variants have proven to be very efficient for nonnegative matrix/tensor factorization issues and outperform many other competitors [39, 43, 44, 45]. In the sequel, we introduce the APG method to solve the coupled nonnegative tensor decomposition problems.

C. Coupled NCPD model

In this study, we mainly consider the coupled NCPD model, given a set of N th-order nonnegative tensors $\mathcal{M}^{(s)} \in \mathbb{R}_+^{I_1 \times I_2 \times \dots \times I_N}$, $s = 1, 2, \dots, S$, the model can be expressed as:

$$\begin{aligned} \mathcal{M}^{(s)} &\approx \hat{\mathcal{M}}^{(s)} = \sum_{r=1}^{R^{(s)}} \lambda_r^{(s)} \mathbf{u}_r^{(1,s)} \circ \mathbf{u}_r^{(2,s)} \circ \dots \circ \mathbf{u}_r^{(N,s)} \\ &= \left[\mathcal{D}^{(s)}; \mathbf{U}^{(1,s)}, \mathbf{U}^{(2,s)}, \dots, \mathbf{U}^{(N,s)} \right], \end{aligned} \quad (6)$$

where $\hat{\mathcal{M}}^{(s)} \in \mathbb{R}_+^{I_1 \times I_2 \times \dots \times I_N}$ denotes the estimation of $\mathcal{M}^{(s)}$. $\mathbf{u}_r^{(n,s)} \in \mathbb{R}_+^{I_n}$ denotes the r th column of mode- n factor matrix of the s th tensor and $\mathbf{U}^{(n,s)} = [\mathbf{u}_1^{(n,s)}, \mathbf{u}_2^{(n,s)}, \dots, \mathbf{u}_{R^{(s)}}^{(n,s)}] \in \mathbb{R}_+^{I_n \times R^{(s)}}$. $\mathcal{D}^{(s)} \in \mathbb{R}_+^{R^{(s)} \times \dots \times R^{(s)}}$ represents the s th core tensor with non-zero entries $\lambda_r^{(s)}$ only on its super-diagonal elements. $\hat{\mathcal{M}}_r^{(s)} = \lambda_r^{(s)} \mathbf{u}_r^{(1,s)} \circ \mathbf{u}_r^{(2,s)} \circ \dots \circ \mathbf{u}_r^{(N,s)}$ is termed as a rank-1 tensor generated by the outer product of $\mathbf{u}_r^{(n,s)}$, $n = 1, 2, \dots, N$, and $\lambda_r^{(s)}$ is used to represent the scaling of rank-1 tensor. The decomposition of each tensor $\mathcal{M}^{(s)}$ can be regarded as decomposing a high-order tensor into a minimal number of rank-1 tensors, and the minimum number $R^{(s)}$ is termed as the rank of the tensor or the number of components.

In coupled NCPD model, we assume that each factor matrix includes two parts and satisfies $\mathbf{U}^{(n,s)} = \begin{bmatrix} \mathbf{U}_C^{(n,s)} & \mathbf{U}_I^{(n,s)} \end{bmatrix}$. $\mathbf{U}_C^{(n,s)} \in \mathbb{R}_+^{I_n \times L_n}$, $0 \leq L_n \leq \min(R^{(s)})$ represents the common information shared by all tensors as $\mathbf{U}_C^{(n,1)} = \dots = \mathbf{U}_C^{(n,S)} = \mathbf{U}_C^{(n)}$, and $\mathbf{U}_I^{(n,s)} \in \mathbb{R}_+^{I_n \times (R^{(s)} - L_n)}$ denotes the individual part corresponding to individual tensor. L_n represents the number of coupled components between tensors in the n th mode.

III. PROPOSED ALGORITHM

This section illustrates how to use APG method or combine APG method and low-rank approximation to solve the coupled NCPD problem. In addition, we give some discussions on the properties of the proposed algorithms as well as some implementation remarks.

A. Coupled NCPD using APG

For the coupled NCPD model, the optimization criterion of Euclidean divergence minimization is adopted to minimize the error between the original and estimated tensors. Therefore, given a set of nonnegative tensors $\mathcal{M}^{(s)}$, $s = 1, 2, \dots, S$, the

objective function of coupled NCPD model can be presented as follows:

$$\begin{aligned} \min_{\mathcal{D}^{(s)}, \mathbf{U}^{(n,s)}} F &\frac{1}{2} \sum_{s=1}^S \left\| \mathcal{M}^{(s)} - \left[\mathcal{D}^{(s)}; \mathbf{U}^{(1,s)}, \dots, \mathbf{U}^{(N,s)} \right] \right\|_F^2 \\ \text{s.t.}, \mathcal{D}^{(s)} &\in \mathbb{R}_+^{R^{(s)} \times \dots \times R^{(s)}}, \mathbf{U}^{(n,s)} \in \mathbb{R}_+^{I_n \times R^{(s)}} \end{aligned} \quad (7)$$

where $\mathbf{U}^{(n,s)} = \begin{bmatrix} \mathbf{U}_C^{(n,s)} & \mathbf{U}_I^{(n,s)} \end{bmatrix}$ and $\mathbf{U}_C^{(n,1)} = \dots = \mathbf{U}_C^{(n,S)} = \mathbf{U}_C^{(n)}$. According to BCD framework, the coupled NCPD problem can be converted into several subproblems by optimizing $\mathcal{D}^{(s)}$ and $\mathbf{U}^{(n,s)}$ alternatively in each iteration. Each subproblem can be regarded as a minimization problem of a continuously differentiable function, which can be solved efficiently by APG method [43, 44, 45]. Next we provide a solution for coupled NCPD problem based on APG method.

First, regarding the solution of core tensor $\mathcal{D}^{(s)}$, we adopt (8) (see it at the top of next page). By keeping all the other variables and using the Lagrange multiplier method, $\mathcal{D}^{(s)}$ can be updated in a closed form as follows:

$$\mathcal{D}^{(s)} = \max \left(0, \hat{\mathcal{D}}^{(s)} - \frac{\hat{\mathcal{G}}^{(s)}}{L_d^{(s)}} \right) \quad (9)$$

where $\hat{\mathcal{D}}^{(s)}$ denotes an extrapolated point and $L_d^{(s)}$ denotes the Lipschitz constant of $F'(\mathcal{D}^{(s)})$. $\hat{\mathcal{G}}^{(s)}$ is the block-partial gradient of (7) at $\hat{\mathcal{D}}^{(s)}$, which can be calculated as:

$$\begin{aligned} \hat{\mathcal{G}}^{(s)} &= \text{ddiag} \left[\left(\mathbf{U}^{(s)T} \mathbf{U}^{(s)} \right)^{\otimes} \text{ddiag} \left(\hat{\mathcal{D}}^{(s)} \right) \right. \\ &\quad \left. - \left(\mathbf{U}^{(s)\odot} \right)^T \text{vec} \left(\mathcal{M}^{(s)} \right) \right] \end{aligned} \quad (10)$$

where $\text{vec}(\mathcal{M}^{(s)})$ denotes the vectorization of tensor $\mathcal{M}^{(s)}$. $\text{ddiag}(\mathcal{D}^{(s)})$ denotes a vector vectorized from the super-diagonal elements of $\mathcal{D}^{(s)}$, and the outer-loop notation $\text{ddiag}(\cdot)$ means the tensorization from a vector to a super-diagonal tensor, which is the reverse operation of the inner-loop $\text{ddiag}(\cdot)$.

Second, for the solution of factor matrix $\mathbf{U}^{(n,s)}$ (without coupled information), we adopt the updating method as (11) (see it at the top of next page), which can be written in the closed form as follows:

$$\mathbf{U}^{(n,s)} = \max \left(0, \hat{\mathbf{U}}^{(n,s)} - \frac{\hat{\mathcal{G}}^{(n,s)}}{L_u^{(n,s)}} \right) \quad (12)$$

where $\hat{\mathbf{U}}^{(n,s)}$ denotes an extrapolated point of $\mathbf{U}^{(n,s)}$, $L_u^{(n,s)}$ denotes a Lipschitz constant of block-partial gradient of (7) at $\mathbf{U}^{(n,s)}$. The block-partial gradient $\hat{\mathcal{G}}^{(n,s)}$ of (7) at $\hat{\mathbf{U}}^{(n,s)}$ is expressed as:

$$\begin{aligned} \hat{\mathcal{G}}^{(n,s)} &= \hat{\mathbf{U}}^{(n,s)} \mathcal{D}^{(s)} \left(\mathbf{U}^{(s)T} \mathbf{U}^{(s)} \right)^{\otimes -n} \mathcal{D}^{(s)} \\ &\quad - \mathcal{M}_{(n)}^{(s)} \mathbf{U}^{(s)\odot -n} \mathcal{D}^{(s)} \end{aligned} \quad (13)$$

where $\mathcal{M}_{(n)}^{(s)}$ denotes the mode- n matricization of $\mathcal{M}^{(s)}$. $\mathcal{D}^{(s)}$ is a diagonal matrix and its diagonal elements correspond to the super-diagonal elements of core tensor $\mathcal{D}^{(s)}$.

$$\mathcal{D}^{(s)} = \underset{\mathcal{D}^{(s)} \geq 0}{\operatorname{argmin}} \left[F(\hat{\mathcal{D}}^{(s)}) + \langle \hat{\mathcal{G}}^{(s)}, \mathcal{D}^{(s)} - \hat{\mathcal{D}}^{(s)} \rangle + \frac{L_d^{(s)}}{2} \left\| \mathcal{D}^{(s)} - \hat{\mathcal{D}}^{(s)} \right\|_F^2 \right] \quad (8)$$

$$\mathbf{U}^{(n,s)} = \underset{\mathbf{U}^{(n,s)} \geq 0}{\operatorname{argmin}} \sum_{s=1}^S \left[F(\hat{\mathbf{U}}^{(n,s)}) + \langle \hat{\mathbf{G}}^{(n,s)}, \mathbf{U}^{(n,s)} - \hat{\mathbf{U}}^{(n,s)} \rangle + \frac{L_u^{(n,s)}}{2} \left\| \mathbf{U}^{(n,s)} - \hat{\mathbf{U}}^{(n,s)} \right\|_F^2 \right] \quad (11)$$

Third, for the factor matrix which includes $\mathbf{U}_C^{(n)}$ and $\mathbf{U}_I^{(n,s)}$, we need to calculate their solutions separately. Since $\mathbf{U}_C^{(n)}$ is shared by all tensors as $\mathbf{U}_C^{(n,1)} = \dots = \mathbf{U}_C^{(n,S)} = \mathbf{U}_C^{(n)}$, we should combine the information of all tensors to calculate the solution of $\mathbf{U}_C^{(n)}$. The solution of individual part $\mathbf{U}_I^{(n,s)}$ only needs to consider the corresponding s -th set tensor. Therefore, we have

$$\mathbf{U}_C^{(n)} = \max \left(0, \hat{\mathbf{U}}_C^{(n)} - \frac{\sum_{s=1}^S \hat{\mathbf{G}}_C^{(n,s)}}{\sum_{s=1}^S L_u^{(n,s)}} \right), \quad (14)$$

and

$$\mathbf{U}_I^{(n,s)} = \max \left(0, \hat{\mathbf{U}}_I^{(n,s)} - \frac{\hat{\mathbf{G}}_I^{(n,s)}}{L_u^{(n,s)}} \right) \quad (15)$$

where $\hat{\mathbf{G}}_C^{(n,s)}$ and $\hat{\mathbf{G}}_I^{(n,s)}$ denote the block-partial gradients of (7) at $\hat{\mathbf{U}}_C^{(n,s)}$ and $\hat{\mathbf{U}}_I^{(n,s)}$, respectively. $\hat{\mathbf{U}}_C^{(n,s)}$ and $\hat{\mathbf{U}}_I^{(n,s)}$ denote the extrapolated points of $\mathbf{U}_C^{(n,s)}$ and $\mathbf{U}_I^{(n,s)}$. Moreover, $\hat{\mathbf{U}}^{(n,s)} = \begin{bmatrix} \hat{\mathbf{U}}_C^{(n,s)} \\ \hat{\mathbf{U}}_I^{(n,s)} \end{bmatrix}$ and $\hat{\mathbf{G}}^{(n,s)} = \begin{bmatrix} \hat{\mathbf{G}}_C^{(n,s)} \\ \hat{\mathbf{G}}_I^{(n,s)} \end{bmatrix}$.

Consider updating $\mathcal{D}^{(s)}$ and $\mathbf{U}^{(n,s)}$ at the k th iteration. The extrapolated points $\hat{\mathcal{D}}_{k-1}^{(s)}$ and $\hat{\mathbf{U}}_{k-1}^{(n,s)}$ are defined as

$$\hat{\mathcal{D}}_{k-1}^{(s)} = \mathcal{D}_{k-1}^{(s)} + w_{d,k-1}^{(s)} \left(\mathcal{D}_{k-1}^{(s)} - \mathcal{D}_{k-2}^{(s)} \right), \quad (16)$$

and

$$\hat{\mathbf{U}}_{k-1}^{(n,s)} = \mathbf{U}_{k-1}^{(n,s)} + w_{u,k-1}^{(n,s)} \left(\mathbf{U}_{k-1}^{(n,s)} - \mathbf{U}_{k-2}^{(n,s)} \right) \quad (17)$$

where $w_{d,k-1}^{(s)}$ and $w_{u,k-1}^{(n,s)}$ denote the extrapolation weights. Since APG is not a monotone method, i.e., $F(k)$ may not be smaller than $F(k-1)$. Therefore, if $F(k) \geq F(k-1)$ after iteration k , an additional re-updating of $\mathbf{U}_k^{(n,s)}$ and $\mathcal{D}_k^{(s)}$ will be taken via $\hat{\mathcal{D}}_{k-1}^{(s)} = \mathcal{D}_{k-1}^{(s)}$ and $\hat{\mathbf{U}}_{k-1}^{(n,s)} = \mathbf{U}_{k-1}^{(n,s)}$. In each iteration, we perform the optimization with the order $\mathcal{D}^{(1)}, \mathcal{D}^{(2)}, \dots, \mathcal{D}^{(S)}$ and $\mathbf{U}^{(1,1)}, \dots, \mathbf{U}^{(1,S)}, \dots, \mathbf{U}^{(N,1)}, \dots, \mathbf{U}^{(N,S)}$, which are alternatively updated one after another until convergence. We term the proposed coupled NCPD algorithm based on APG update as CoNCPD-APG and summarize it in Algorithm 1. The detailed derivations and relevant parameter settings are given in the Appendix A.

B. Coupled NCPD using APG and low-rank approximation

In CoNCPD-APG algorithm, the time-consumption of updating $\mathcal{D}^{(s)}$ and $\mathbf{U}^{(n,s)}$ is mainly attributed to the multiplication of $(\mathbf{U}^{(s)\odot})^T \operatorname{vec}(\mathcal{M}^{(s)})$ and $\mathcal{M}_{(n)}^{(s)} \mathbf{U}^{(s)\odot-n}$ in (10) and (13), and it will be increasingly serious especially for the tensors with large dimensionality. Specifically,

Algorithm 1: CoNCPD-APG algorithm

Input: $\mathcal{M}^{(s)}$, L_n and $R^{(s)}$, $n=1, \dots, N$, $s=1, \dots, S$

- 1 Initialization:
- 2 $\mathbf{U}^{(n,s)}$, $\mathcal{D}^{(s)}$, $\mathcal{M}_{(n)}^{(s)}$, $n=1, \dots, N$, $s=1, \dots, S$
- 3 **for** $k=1, 2, \dots, \text{MaxIt}$ **do**
- 4 **for** $s=1, \dots, S$ **do**
- 5 Calculate $\hat{\mathcal{G}}_{k-1}^{(s)}$ and $\hat{\mathcal{D}}_{k-1}^{(s)}$ via (10) and (16)
- 6 Update $\mathcal{D}_k^{(s)}$ via (9)
- 7 **end**
- 8 **for** $n=1, 2, \dots, N$ **do**
- 9 **for** $s=1, \dots, S$ **do**
- 10 Calculate $\hat{\mathbf{G}}_{k-1}^{(n,s)}$ and $\hat{\mathbf{U}}_{k-1}^{(n,s)}$ via (13) and (17)
- 11 Update $\mathbf{U}_k^{(n,s)}$ via (12), (14) and (15)
- 12 **end**
- 13 **end**
- 14 **if** $F(k) \geq F(k-1)$ **then**
- 15 $\hat{\mathcal{D}}_{k-1}^{(s)} = \mathcal{D}_{k-1}^{(s)}$, $\hat{\mathbf{U}}_{k-1}^{(n,s)} = \mathbf{U}_{k-1}^{(n,s)}$
- 16 Reupdate $\mathcal{D}_k^{(s)}$, $\mathbf{U}_k^{(n,s)}$ via (9), (12), (14) and (15)
- 17 **end**
- 18 **if** *stopping criterion is satisfied* **then**
- 19 **return**
- 20 $\mathbf{U}_k^{(n,s)}$, $\mathcal{D}_k^{(s)}$, $n=1, \dots, N$, $s=1, \dots, S$
- 21 **end**
- 22 **end**

Output: $\mathbf{U}^{(n,s)}$, $\mathcal{D}^{(s)}$, $n=1, \dots, N$, $s=1, \dots, S$

in each iteration, let $R^{(s)} = R$, the computational complexity of $(\mathbf{U}^{(s)\odot})^T \operatorname{vec}(\mathcal{M}^{(s)})$ reaches $\mathcal{O}(SR \prod_n I_n)$ and $\mathcal{M}_{(n)}^{(s)} \mathbf{U}^{(s)\odot-n}$ has the complexity of $\mathcal{O}(NSR \prod_n I_n)$. The applications of low-rank approximation in nonnegative matrix/tensor factorization have demonstrated their performance improvement in terms of computational efficiency while maintaining computational accuracy [38, 39, 46]. Generally, the unconstrained CPD of a tensor converges in dozens of iterations and is considered faster than its counterpart with nonnegative constraint. Therefore, to reduce the computational complexity of CoNCPD-APG algorithm, we consider introducing the low-rank approximation of $\mathcal{M}^{(s)}$ before performing the actual coupled decomposition. Suppose that $\left[\tilde{\mathbf{U}}^{(1,s)}, \tilde{\mathbf{U}}^{(2,s)}, \dots, \tilde{\mathbf{U}}^{(N,s)} \right]$ is the rank- $\tilde{R}^{(s)}$ approximation of $\mathcal{M}^{(s)}$ obtained by the unconstrained CPD, $\tilde{\mathbf{U}}^{(n,s)} \in \mathbb{R}^{I_n \times \tilde{R}^{(s)}}$, $\tilde{R}^{(s)} \leq R^{(s)}$, thus the cost function in (7) can be re-

represented as the optimization problem in (18) (see it at the top of next page) with fixed $\tilde{U}^{(1,s)}, \tilde{U}^{(2,s)}, \dots, \tilde{U}^{(N,s)}$. In other words, instead of loading the original tensor $\mathcal{M}^{(s)}$ directly into the iterations, we first split the tensor into smaller compressed matrices, such as $\tilde{U}^{(1,s)}, \tilde{U}^{(2,s)}, \dots, \tilde{U}^{(N,s)}$, and then bring them into the decomposition iterations, which can greatly reduce the time and space complexities of algorithms[38]. Via low-rank approximation, $\text{vec}(\mathcal{M}^{(s)})$ and $\mathcal{M}_{(n)}^{(s)}$ in (10) and (13) can be respectively expressed by $\text{vec}(\mathcal{M}^{(s)}) = \tilde{U}^{(s)\odot} \text{ddiag}(\mathcal{I})$ and $\mathcal{M}_{(n)}^{(s)} = \tilde{U}^{(s,n)} (\tilde{U}^{(s)\odot-n})^T$, and $\mathcal{I} \in \mathbb{R}^{\tilde{R}^{(s)} \times \dots \times \tilde{R}^{(s)}}$ denotes a core tensor with all super-diagonal elements being 1. This thereby leads to

$$\begin{aligned}
 \left(\mathbf{U}^{(s)\odot}\right)^T \text{vec}\left(\mathcal{M}^{(s)}\right) &= \left(\mathbf{U}^{(s)\odot}\right)^T \tilde{U}^{(s)\odot} \text{ddiag}(\mathcal{I}) \\
 &= \left(\mathbf{U}^{(s)T} \tilde{U}^{(s)}\right)^{\otimes} \text{ddiag}(\mathcal{I})
 \end{aligned} \quad (19)$$

and

$$\begin{aligned}
 \mathcal{M}_{(n)}^{(s)} \mathbf{U}^{(s)\odot-n} &= \tilde{U}^{(s,n)} \left(\tilde{U}^{(s)\odot-n}\right)^T \mathbf{U}^{(s)\odot-n} \\
 &= \tilde{U}^{(s,n)} \left(\tilde{U}^{(s)T} \mathbf{U}^{(s)}\right)^{\otimes-n}.
 \end{aligned} \quad (20)$$

By virtue of low-rank approximation, only very small matrices are involved to perform the multiplications in (20) and (19). In addition, the computational complexities of $\left(\mathbf{U}^{(s)\odot}\right)^T \text{vec}(\mathcal{M}^{(s)})$ and $\mathcal{M}_{(n)}^{(s)} \mathbf{U}^{(s)\odot-n}$ are respectively reduced to $\mathcal{O}(SR\tilde{R} \sum_n I_n)$ and $\mathcal{O}(NSR\tilde{R} \sum_n I_n)$ via the transformation of (19) and (20) (here we set $\tilde{R}^{(s)} = \tilde{R}$).

Overall, to develop an efficient coupled tensor decomposition algorithm, we further propose the IraCoNCPD-APG algorithm based on CoNCPD-APG algorithm and low-rank approximation. The implementation of IraCoNCPD-APG algorithm includes two steps: (i) performing unconstrained CPD of tensors $\mathcal{M}^{(s)}$ successively to achieve their low-rank approximation as $\mathcal{M}^{(s)} \approx \left[\tilde{U}^{(1,s)}, \tilde{U}^{(2,s)}, \dots, \tilde{U}^{(N,s)}\right]$; (ii) updating $\mathbf{U}_k^{(n,s)}$ and $\mathcal{D}_k^{(s)}$ via solving the optimization problem in (18) with fixed $\tilde{U}^{(1,s)}, \tilde{U}^{(2,s)}, \dots, \tilde{U}^{(N,s)}$. The framework of IraCoNCPD-APG algorithm is presented in Algorithm 2.

Algorithm 2: larCoNCPD-APG algorithm

Input: $\mathcal{M}^{(s)}$, L_n , and $R^{(s)}$, $n = 1, \dots, N$,
 $s = 1, \dots, S$

- 1 Initialization:
 - 2 $\mathbf{U}^{(n,s)}$, $\mathcal{D}^{(s)}$, $\mathcal{M}_{(n)}^{(s)}$, $n = 1, \dots, N$, $s = 1, \dots, S$
 - 3 Calculate $\tilde{U}^{(n,s)}$, $n = 1, \dots, N$, $s = 1, \dots, S$ via unconstrained CPD on $\mathcal{M}^{(s)}$, $s = 1, \dots, S$
 - 4 **for** $k = 1, 2, \dots, \text{MaxIt}$ **do**
 - 5 Repeat the 4th to 21st command lines of Algorithm 1 except the 5th and 10th lines:
 - 6 Calculate $\hat{\mathcal{G}}_{k-1}^{(s)}$ and $\hat{\mathcal{G}}_{k-1}^{(n,s)}$ via (10) and (13) by introducing (19) and (20)
 - 7 **end**
- Output:** $\mathbf{U}^{(n,s)}$, $\mathcal{D}^{(s)}$, $n = 1, \dots, N$, $s = 1, \dots, S$
-

C. Remarks and discussion

1) *Exact&flexible coupling:* The coupled NCPD models in (6) consider the exact coupling through a common part which has to be shared by all the tensors $\mathcal{M}^{(s)}$ as $\mathbf{U}_C^{(n,1)} = \mathbf{U}_C^{(n,2)} = \dots = \mathbf{U}_C^{(n,S)}$. Although the coupling assumption is relatively restrictive, the models can also flexibly depict the connections between tensors to some extent. For example, we can impose couplings on any modes or some of them, and the coupling on every mode can be partial or complete. More interestingly, the couplings can be imposed only on specific tensors, and it's easy to derive formulas and modify the code from our work. Please refer to [47] for more flexibly linear couplings, which will be one of our works.

2) *Removal of core tensors:* In NCPD, core tensor \mathcal{D} is generally merged into the factor matrices that can slightly reduce the computation load. Analogously, we can extend this means to the coupled NCPD, but only for the case where all N modes are not fully coupled among tensors [11], i.e., $\exists n$ leading to $L_n = 0$. However, for the cases that $\forall n$, $L_n > 0$, the core tensors $\mathcal{D}^{(s)}$ are required and used to differentiate the magnitude of corresponding components (rank-1 tensor) among tensors. In Experiment 1, we design the coupled NCPD problem using synthetic data and verify the importance of core tensors in some cases. In Experiment 3, the scaling features of corresponding brain activities provided by core tensors extracted from ERP tensors are used to classify the groups of patients and healthy controls. Thus, the removal of core tensors depends on the coupling constraints on the tensor data.

3) *Computational complexity:* For the computational complexity, we mainly calculate the time complexity based on the multiplication operations. From Section III, the computational load is mostly dominated by the updates of $\mathcal{D}^{(s)}$ and $\mathbf{U}^{(n,s)}$, especially the calculation of block-partial gradients $\hat{\mathcal{G}}^{(s)}$ and $\hat{\mathcal{G}}^{(n,s)}$ in (10) and (13). The costs of calculating them (n th mode of s th tensor) per iteration are listed in Table II. Let $R^{(s)} = R$, considering there are N modes and S tensors, the total time complexity for each iteration of CoNCPD-APG algorithm reaches $\mathcal{O}(NSR \prod_{n=1}^N I_n)$. By introducing low-rank approximation, (10) and (13) can be calculated using (19) and (20), the costs of which are also given in Table II. Let $\tilde{R}^{(s)} = R$, the overall computation load per iteration of IraCoNCPD-APG algorithm is reduced to $\mathcal{O}(NSR^2 \sum_{n=1}^N I_n)$.

4) *Error bound and convergence analysis:* Inspired by [38], we also examined the cost and error of low-rank approximation brought for the results of the whole steps.

Proposition 1: For a series of tensors $\mathcal{Y}^{(s)} \in \mathbb{R}^{I_1 \times I_2 \times \dots \times I_N}$, suppose that there are nonnegative factor matrices $\mathbf{U}_{\diamond}^{(n,s)}$ ($s \leq S$, $n \leq N$ in this part) satisfying $\{\mathbf{U}_{\diamond}^{(1,s)}, \mathbf{U}_{\diamond}^{(2,s)}, \dots, \mathbf{U}_{\diamond}^{(N,s)}\} =$

$\underset{\mathbf{U}^{(n,s)} \geq 0}{\text{argmin}} \sum_{s=1}^S \left\| \mathcal{Y}^{(s)} - \left[\mathbf{U}^{(1,s)}, \mathbf{U}^{(2,s)}, \dots, \mathbf{U}^{(N,s)}\right] \right\|_F$. Let $\left\| \mathcal{Y}^{(s)} - \left[\mathbf{U}_{\diamond}^{(1,s)}, \mathbf{U}_{\diamond}^{(2,s)}, \dots, \mathbf{U}_{\diamond}^{(N,s)}\right] \right\|_F = \epsilon_{\diamond}^{(s)}$ and $\mathcal{X}^{(s)} = \left[\tilde{U}^{(1,s)}, \tilde{U}^{(2,s)}, \dots, \tilde{U}^{(N,s)}\right]$ be the low-rank approximation (e.g., unconstrained CPD) to $\mathcal{Y}^{(s)}$, then we have

$$\text{(i) } \min_{\mathbf{U}^{(n,s)} \geq 0} \sum_{s=1}^S \left[\left\| \mathcal{Y}^{(s)} - \mathcal{X}^{(s)} \right\|_F + \left\| \mathcal{X}^{(s)} - \left[\mathbf{U}^{(1,s)}, \dots, \mathbf{U}^{(N,s)}\right] \right\|_F \right] = \sum_{s=1}^S \epsilon_{\diamond}^{(s)}.$$

$$\min_{\mathcal{D}^{(s)}, \mathcal{U}^{(n,s)}} \mathcal{F} \frac{1}{2} \sum_{s=1}^S \left\| \left[\tilde{\mathcal{U}}^{(1,s)}, \tilde{\mathcal{U}}^{(2,s)}, \dots, \tilde{\mathcal{U}}^{(N,s)} \right] - \left[\mathcal{D}^{(s)}; \mathcal{U}^{(1,s)}, \mathcal{U}^{(2,s)}, \dots, \mathcal{U}^{(N,s)} \right] \right\|_F^2 \quad (18)$$

s.t. $\mathcal{D}^{(s)} \in \mathbb{R}_+^{I_1 \times \dots \times I_N}$, $\mathcal{U}^{(n,s)} \in \mathbb{R}_+^{I_n \times R^{(s)}}$, $\tilde{\mathcal{U}}^{(n,s)} \in \mathbb{R}^{I_n \times \tilde{R}^{(s)}}$, $\tilde{R}^{(s)} \leq R^{(s)}$

TABLE II
TIME COMPLEXITY PER ITERATION IN CoNCPD-APG AND IraCoNCPD-APG ALGORITHMS: n TH MODE OF s TH TENSOR

Equation	Operation	Description	Input size	Output size	Cost
(10)	① = $(\mathcal{U}^{(s)T} \mathcal{U}^{(s)})^\circledast$	Hadamard product	$I_n \times R, n = 1, 2, \dots, N$	$R \times R$	$R^2 \sum_{n=1}^N I_n + R^2 N$
(10)	② = $(\mathcal{U}^{(s)\circledast})^T$	Khatri-Rao product	$I_n \times R, n = 1, 2, \dots, N$	$R \times \prod_{n=1}^N I_n$	$R \prod_{n=1}^N I_n$
(10)	③ = ② · $\text{vec}(\mathcal{M}^{(s)})$	Matrix product	$R \times \prod_{n=1}^N I_n, \prod_{n=1}^N I_n \times 1$	$R \times 1$	$R \prod_{n=1}^N I_n$
(13)	④ = $(\mathcal{U}^{(s)T} \mathcal{U}^{(s)})^\circledast^{-n}$	Hadamard product	$I_m \times R, m = 1, \dots, N, m \neq n$	$R \times R$	$R^2 \sum_{m \neq n}^N I_m + R^2(N-1)$
(13)	⑤ = $\tilde{\mathcal{U}}^{(n,s)} \cdot \textcircled{4}$	Matrix product	$I_n \times R, R \times R$	$I_n \times R$	$R^2 I_n$
(13)	⑥ = $\mathcal{U}^{(s)\circledast^{-n}}$	Khatri-Rao product	$I_m \times R, m = 1, \dots, N, m \neq n$	$\prod_{m \neq n}^N I_m \times R$	$R \prod_{m \neq n}^N I_m$
(13)	⑦ = $\mathcal{M}^{(s)} \cdot \textcircled{6}$	Matrix product	$I_n \times \prod_{m \neq n}^N I_m, \prod_{m \neq n}^N I_m \times R$	$I_n \times R$	$R \prod_{n=1}^N I_n$
(19)	⑧ = $(\mathcal{U}^{(s)T} \tilde{\mathcal{U}}^{(s)})^\circledast$	Hadamard product	$I_n \times R, n = 1, 2, \dots, N$	$R \times R$	$R^2 \sum_{n=1}^N I_n + R^2 N$
(20)	⑨ = $(\tilde{\mathcal{U}}^{(s)T} \mathcal{U}^{(s)})^\circledast^{-n}$	Hadamard product	$I_m \times R, m = 1, \dots, N, m \neq n$	$R \times R$	$R^2 \sum_{m \neq n}^N I_m + R^2(N-1)$
(20)	⑩ = $\tilde{\mathcal{U}}^{(s,n)} \cdot \textcircled{9}$	Matrix product	$I_n \times R, R \times R$	$I_n \times R$	$R^2 I_n$

¹ Here let $R^{(s)} = \tilde{R}^{(s)} = R, s = 1, 2, \dots, S$.

(ii) If $\left\| \mathcal{Y}^{(s)} - \mathcal{X}^{(s)} \right\|_F = \theta^{(s)}$, suppose that there are nonnegative factor matrices $\tilde{\mathcal{U}}^{(n,s)}$ ($s \leq S, n \leq N$ in this part) satisfying $\left\{ \tilde{\mathcal{U}}^{(1,s)}, \tilde{\mathcal{U}}^{(2,s)}, \dots, \tilde{\mathcal{U}}^{(N,s)} \right\} = \text{argmin}_{\tilde{\mathcal{U}}^{(n,s)} \geq 0} \sum_{s=1}^S \left\| \mathcal{X}^{(s)} - \left[\mathcal{U}^{(1,s)}, \mathcal{U}^{(2,s)}, \dots, \mathcal{U}^{(N,s)} \right] \right\|_F$. Then $\sum_{s=1}^S \epsilon_s^\diamond \leq \sum_{s=1}^S \left\| \mathcal{Y}^{(s)} - \left[\tilde{\mathcal{U}}^{(1,s)}, \tilde{\mathcal{U}}^{(2,s)}, \dots, \tilde{\mathcal{U}}^{(N,s)} \right] \right\|_F \leq \sum_{s=1}^S \left[2\theta^{(s)} + \epsilon_s^\diamond \right]$.

The proof of **Proposition 1** can be found in Appendix B.

Under BCD framework, the objective function of coupled NCPD model in (7) was converted into two alternative sets of continuously differentiable functions as in (8) and (11). Each function is a convex function with Lipschitz continuous gradient, and the solution will be converged to a stationary point as an optimal convergence rate of $\mathcal{O}(\frac{1}{K^2})$, which has been thoroughly demonstrated in [41, 43, 44] and will not be further analyzed in this study.

5) *Termination criteria*: For the stopping criteria during algorithm optimization, we consider two parameters: the change of average relative error (RelErr) and the maximum number of iterations (MaxIt). We define

$$\text{RelErr} \triangleq \frac{1}{S} \sum_{s=1}^S \left[\left\| \mathcal{M}^{(s)} - \hat{\mathcal{M}}^{(s)} \right\|_F / \left\| \mathcal{M}^{(s)} \right\|_F \right] \quad (21)$$

where $\mathcal{M}^{(s)}$ and $\hat{\mathcal{M}}^{(s)}$ are the original and recovered tensors. Furthermore, we stipulate $|\text{RelErr}_{\text{new}} - \text{RelErr}_{\text{old}}| < \varepsilon$, i.e., the adjacent RelErr change should be smaller than the preselected threshold. In this study, we choose $\varepsilon = 1e-8$ and MaxIt=1000 for the coupled algorithms, and $\varepsilon = 1e-4$ and MaxIt=200 for the low-rank approximation.

6) *Component number selection*: In terms of the number of components and coupled components, i.e., $\tilde{R}^{(s)}$, $R^{(s)}$ and L_n , we set ground-truth values for the synthetic experiment. For the real-world data, we adopt the principal component analysis

(PCA) method, and the number of principal components with 99% explained variance is selected as the number of components. Considering that the nonnegative rank is generally no less than the ordinary rank, so we set $\tilde{R}^{(s)} = R^{(s)}$ in this study [38]. Inspired by the tensor spectral clustering method proposed in [48] and the matlab toolbox¹, we calculate the number of coupled components L_n as: if components from at least half of the tensors have a fairly high correlation coefficient, e.g., 0.7, we consider them as the coupled components.

IV. EXPERIMENTS AND RESULTS

In this section, we design and perform three experiments on synthetic data, face image data and two kinds of real-world electroencephalography (EEG) data, aiming to examine and demonstrate the superior performance of CoNCPD-APG and IraCoNCPD-APG algorithms on the coupled NCPD problem.

Experiment settings: We use alternating least squares (ALS, [4]) algorithm to implement the low-rank approximation, which has proven to be a reasonable solver for unconstrained CPD problems [39]. The optimization strategies including fast hierarchical alternating least squares (fHALS, [29, 49, 50]), multiplicative updating (MU, [51, 52]), alternating direction method of multipliers (ADMM, [28, 53]) and ALS are used as the competitors to the proposed algorithms. For performance comparison, (1) we adopt model fit to evaluate the reconstructed error between original and recovered tensors via $\text{Fit} \triangleq \frac{1}{S} \sum_s \left[1 - \left\| \mathcal{M}^{(s)} - \hat{\mathcal{M}}^{(s)} \right\|_F / \left\| \mathcal{M}^{(s)} \right\|_F \right]$; (2) we record the running time to access the utility of the low-rank approximation; (3) we adopt the performance index (PI)

¹https://github.com/GHu-DUT/Tensor_Spectral_Clustering

to measure the accuracy of recovered factor matrices via

$$\text{PI} \triangleq \frac{1}{2R(R-1)} \left[\sum_{i=1}^R \left(\sum_{j=1}^R \frac{|g_{ij}|}{\max_k |g_{ik}|} \right) + \sum_{i=1}^R \left(\sum_{j=1}^R \frac{|g_{ji}|}{\max_k |g_{ki}|} \right) \right], \quad (22)$$

where g_{ij} denotes the (i, j) th element of the matrix $\mathbf{G} = \tilde{\mathbf{U}}^\dagger \mathbf{U}$. $\tilde{\mathbf{U}}$ is the estimation of the factor matrix \mathbf{U} , and \dagger denotes the pseudo inverse operator. The small value of PI indicates an accurate estimation of the true factor matrix regardless of scale and permutation ambiguity. The input factor matrices and core tensors are initialized with uniformly distributed pseudorandom numbers generated by MATLAB function `rand`. Signal-to-noise ratio (SNR) is defined as $\text{SNR} = 10 \log_{10}(p_s/p_n)$, where p_s and p_n are the signal and noise levels. Then the noise can be added to each tensor as

$$\mathcal{M}_{\text{noise}} = p_s \mathcal{M} + p_n \frac{\mathcal{N}}{\|\mathcal{N}\|} \|\mathcal{M}\|_F, \quad (23)$$

where \mathcal{N} is the noise whose entries are drawn from standard normal distribution.

The experiments were carried out with the following computer configurations: CPU-Intel Core i9-14900KF @3.20 GHz; Memory-128 GB; System-64-bit Windows 11; Software-MATLAB R2022b.

A. Experiment 1 Synthetic data

In this experiment, we design detailed experiments to illustrate the performance of CoNCPD-APG and lraCoNCPD-APG algorithms in terms of decomposition efficiency and accuracy using synthetic data. First, we simulated 20 third-order tensors that are partially/fully coupled in one, two, or three modes according to equation (6). Second, we compare the performance using different levels of noise and tensor sizes. Last, we design some special cases to compare the performance of proposed algorithms with and without core tensors. For each experiment, the sizes of tensors are given as $I_{1,2,3} = [100, 100, 100]$ (except for Exp. 1e, which has varying tensor sizes). The rank of tensors is set to 10, meaning that the ground-truth non-negative factor matrices have 10 components, whose entries are drawn from the uniform distribution. For the noise, we apply a fixed SNR of 20 dB, except for Exp. 1d, which has multiple noise levels. To ensure the reliability of the algorithms, we perform 100 independent runs for each simulation and report the average results.

a) Experiment 1a: coupled in three modes: First, we set the number of coupled components as $L_{1,2,3} = [10, 10, 10]$ and $[5, 5, 5]$, corresponding to the fully coupled or partially coupled cases.

b) Experiment 1b: coupled in two modes: Then, we consider the coupled cases in two modes, and the number of coupled components among tensors is set to $L_{1,2,3} = [10, 10, 0]$ and $[5, 5, 0]$.

c) Experiment 1c: coupled in one mode: Here we examine the coupled cases in one mode, where the number of coupled components among tensors is specified as $L_{1,2,3} = [10, 0, 0]$ and $[5, 0, 0]$.

For the first three simulation experiments, from TABLE III, we can see that all algorithms perform almost identically

TABLE III
PERFORMANCE COMPARISON OF THE ALGORITHMS FOR TENSOR MODELS THAT ARE COUPLED IN ONE, TWO, AND THREE MODES OPTIMIZED USING DIFFERENT ALGORITHMS (THE VALUES IN THE ROW * ARE THE PERFORMANCE OF TWO STEPS IN THE LRACoNCPD-APG ALGORITHM)

Settings	Experiment 1a		Experiment 1b		Experiment 1c		
	$L_{1,2,3}$	[10,10,10]	[5,5,5]	[10,10,0]	[5,5,0]	[10,0,0]	[5,0,0]
Fit	ADMM	0.9534	0.9528	0.9536	0.9536	0.9535	0.9536
	MU	0.9534	0.9484	0.9526	0.9532	0.9525	0.9527
	ALS	0.9507	0.9534	0.9534	0.9535	0.9517	0.9534
	fHALS	0.9534	0.9531	0.9536	0.9536	0.9533	0.9535
	APG	0.9534	0.9524	0.9536	0.9536	0.9531	0.9535
	lra&APG	0.9522	0.9492	0.9529	0.9526	0.9522	0.9521
	*step1	0.9488	0.9488	0.9515	0.9517	0.9514	0.9515
	*step2	0.9799	0.9852	0.9886	0.9909	0.9887	0.9914
	ADMM	0.0040	0.0185	0.0039	0.0043	0.0041	0.0042
	ALS	0.0087	0.0069	0.0045	0.0049	0.0110	0.0059
PI	MU	0.0040	0.0593	0.0183	0.0093	0.0188	0.0147
	fHALS	0.0039	0.0092	0.0045	0.0054	0.0055	0.0059
	APG	0.0039	0.0199	0.0040	0.0043	0.0055	0.0042
	lra&APG	0.0079	0.0500	0.0113	0.0124	0.0152	0.0185
	ADMM	15.993	19.387	9.1603	9.3587	9.9832	9.2803
Time	ALS	5.8274	5.5828	2.9349	2.4715	3.8710	2.8685
	MU	51.409	38.017	19.834	22.979	20.789	20.298
	fHALS	6.8604	12.200	7.7722	3.4584	8.5071	6.7957
	APG	8.5072	18.440	5.2630	5.6902	5.6701	5.9041
	lra&APG	1.4356	2.1844	1.0896	1.0934	1.1867	1.2285
	*step1	0.7959	0.6381	0.5381	0.5360	0.5757	0.5688
	*step2	0.6397	1.5463	0.5515	0.5574	0.6110	0.6598

on the tensor fitting values for various coupled types. From the perspective of PI values and running time, except for the second coupling type in Experiment 1a, the proposed CoNCPD-APG algorithm is very competitive in terms of both decomposition speed and accuracy of the recovered factor matrix. Although the ALS-based algorithm runs faster than others, its decomposition accuracy for factor matrices is slightly lower, indicating that the convergence is not thorough enough. Conversely, while the ADMM-based algorithm converges slowly, it achieves high decomposition accuracy. For the proposed lraCoNCPD-APG algorithm, both the unconstrained ALS and APG optimization steps converge rapidly, achieving high tensor fitting and accurate estimation of the factor matrices. Compared to methods without low-rank approximation, our approach achieves convergence 5 to 10 times faster with only a minimal loss in decomposition precision.

d) Experiment 1d: different noises: In this scenario, we demonstrate and compare the performance of the proposed algorithms across a range of SNR values (from 0 to 20dB with steps of 2dB) under the following settings: partially coupled in two modes as $L_{1,2,3} = [5, 5, 0]$.

As can be seen from Fig. 1, all algorithms exhibit very similar performance in terms of tensor fit across the range of SNR values. Regarding PI values, all algorithms perform comparably at high SNRs. However, the CoNCPD-APG algorithm outperforms the others at low SNRs, while ranking in the middle in terms of running time. The introduction of

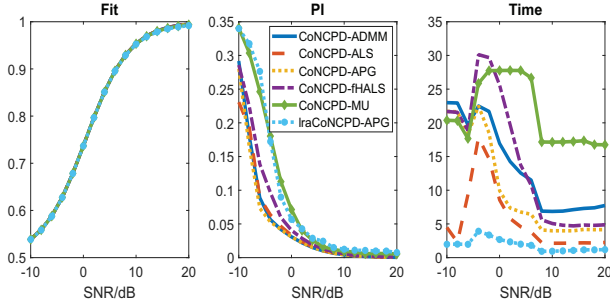


Fig. 1. Performance comparison of CoNCPD-APG, IraCoNCPD-APG, and their competitors at different additive noise levels

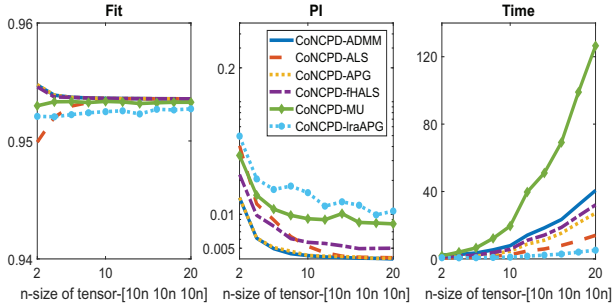


Fig. 2. Performance comparison of CoNCPD-APG, IraCoNCPD-APG, and their competitors using different tensor sizes

LRA greatly improves the running speed, though it slightly compromises decomposition accuracy.

e) Experiment 1e: different sizes: To evaluate the decomposition performance with varying tensor sizes, we define the tensor dimensions as $I_{1,2,3} = [10n, 10n, 10n]$, where n ranges from 1 to 20 with steps of 2. We adopt the case with partially coupled data across two modes $L_{1,2,3} = [5, 5, 0]$.

In this case, the change in tensor size has little effect on the tensor fit, but as the tensor size increases, the PI value becomes smaller and the running time becomes significantly longer, as shown in Fig. 2. The CoNCPD-APG and CoNCPD-ADMM algorithms have similar performance in terms of PI values, while CoNCPD-APG takes less time to run. With LRA, IraCoNCPD-APG can greatly reduce the execution time, and this advantage becomes more significant as the size of tensors increases. Meanwhile, its cost is only a slight reduction in decomposition accuracy.

f) Experiment 1f: core tensors or not: As discussed in III-C2, the core tensors are necessary for the cases that $\forall n, L_n > 0$. Here we take the case of $L_{1,2,3} = [5, 5, 5]$ as an example, and the algorithms without optimizing core tensors are respectively termed as CoNCPD-APG-NC and IraCoNCPD-APG-NC.

From Fig. 3, we can see that CoNCPD-APG achieves the best decomposition accuracy on PI values, followed by IraCoNCPD-APG, CoNCPD-APG-NC and IraCoNCPD-APG-NC. It should be noted that the tensor fitting curve of IraCoNCPD-based algorithms is drawn from its second step, which is why it is higher than CoNCPD-based algorithms. This is only to illustrate that the convergence accuracy of the second step of the algorithm is still relatively high. Actually,

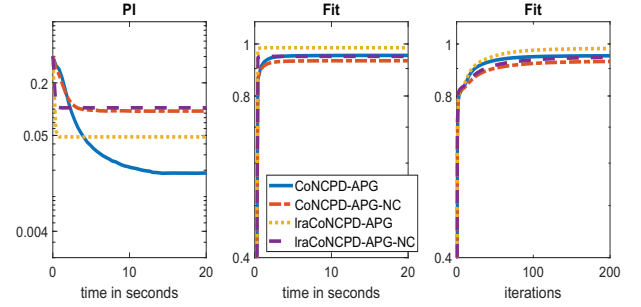


Fig. 3. Performance comparison of CoNCPD-APG, IraCoNCPD-APG, CoNCPD-APG-NC, and IraCoNCPD-APG-NC algorithms.

for IraCoNCPD-APG algorithm, the final global tensor fit is 0.9, which is lower than 0.95 of CoNCPD-APG, followed by CoNCPD-APG-NC with 0.85 and IraCoNCPD-APG-NC with 0.8. To sum up, the core tensors are required in some cases.

B. Experiment 2 Face image data

In this experiment, we conduct coupled tensor decomposition analysis using the extended Yale B face database² for image reconstruction and denoising. This database contains gray-scale face images of 38 subjects acquired from 9 poses and 64 illumination conditions, here we only use the cropped images under frontal pose of all illuminations³[54, 55]. In this case, each subject corresponds to 64 images, and each image is cropped and resized to 32×32 pixels. Finally, we have 31 third-order tensors with the size of 32 pixels \times 32 pixels \times 64 condition by stacking face images of each subject along illumination conditions (7 subjects are removed due to data incompleteness). Using the PCA-based method, the component number of tensors for 31 subjects are separately selected as $\{24, 23, 23, 24, 23, 24, 24, 23, 22, 24, 23, 24, 22, 23, 23, 24, 23, 24, 23, 23, 26, 23, 23, 24, 23, 23, 23, 24, 25, 22, 23, 22, 22, 23, 24, 24, 25, 23\}$. Specifically, through unfolding along the first mode, each tensor is converted into a matrix with the size of 32×2048 . Then performing the PCA on the matrices successively, and the number of principal components with a total explained variance exceeds 99% is regarded as the corresponding component number. Using the tensor spectral clustering method [48], we select those components that have a correlation value greater than 0.7 and from at least 70% of the tensors as coupled components, and finally 15 coupled components among tensors are extracted.

The performance of the proposed algorithms is compared with their competitors at two noise levels: 0.1 and 0.0001 salt-and-pepper noise. Here we use the matlab function `imnoise` with the parameter `salt & pepper` to add the noise. Peak-signal-to-noise ratio (PSNR) is also used to evaluate the quality of reconstructed face images. Table IV gives the algorithm performance comparison averaged from 100 independent runs. We can see that the proposed APG-based algorithms perform slightly better than other algorithms in tensor fittings and PSNR, indicating high decomposition accuracy and stronger

²<http://vision.ucsd.edu/~leekc/ExtYaleDatabase/ExtYaleB.html>

³<http://www.cad.zju.edu.cn/home/dengcai/Data/FaceData.html>

TABLE IV
PERFORMANCE COMPARISON OF THE ALGORITHMS IN THE IMAGE RECONSTRUCTION AND DENOISING BASED ON COUPLED NCPD MODEL

Settings	Noise=0.1			Noise=0.0001		
	Fit	Time	PSNR	Fit	Time	PSNR
ADMM	0.5053	37.015	21.134	0.7688	36.662	22.066
ALS	0.4940	30.652	20.149	0.7193	34.510	20.354
MU	0.5064	26.062	21.324	0.7773	26.634	22.413
fHALS	0.5028	31.358	20.954	0.7583	29.535	21.691
APG	0.5079	32.830	21.480	0.7816	30.308	22.596
Ira&APG	0.5061	8.708	21.396	0.7794	8.6834	22.504
*step1	0.4938	0.5285	-	0.8353	1.0323	-
*step2	0.8266	8.2146	-	0.8464	7.6512	-

image reconstruction capabilities. More importantly, by introducing low-rank approximation strategy, the IraCoNCPD-APG algorithm can greatly reduce execution time while maintaining decomposition performance.

The execution time of Ira-based algorithm showed in the table includes the running time of the unconstrained CPD and APG optimization, and we also give the performance of each separate step. In addition, Figure 4 gives an illustration of original, noisy, and recovered face images, as well as common and individual face image features obtained by CoNCPD-APG algorithm. The fourth row of images are only common features among different images, while the fifth row is the common features multiplied by the values from core tensors, and the last row is the individual features corresponding to the particular images.

C. Experiment 3 Real-world ERP data

In this experiment, we compare the proposed CoNCPD-APG and IraCoNCPD-APG algorithms with CoNCPD-MU, CoNCPD-fHALS and CoNCPD-MU algorithms in the multi-domain feature extraction of event-related potential (ERP) data⁴. Two groups of data are chosen: 21 children with reading disability (RD) and 21 children with attention deficit (AD), aiming to acquire multi-domain features of ERP data which can better discriminate the two groups. Using complex Morlet wavelet transform, we generate the third-order tensors of 42 subjects (21 RD & 21 AD) with the size of 9 (channels) \times 71 (frequency bins) \times 60 (temporal points) to testify the effectiveness and practicality of coupled tensor decomposition. Following [56], we set the number of components to $R^{(1)} = R^{(2)} = \dots R^{(42)} = 36$. Considering the nature of ERP data, we assume that these third-order ERP tensors are coupled in spatial, spectral and temporal modes, and we directly set the number of coupled components to 36.

ERP data are acquired through repeated presentation of stimuli, which makes their properties in temporal, spectral and spatial domains roughly known before they are actually extracted. According to prior knowledge given in [56], we can select the expected multi-domain features and their corresponding temporal, spectral and spatial components from the

TABLE V
PERFORMANCE COMPARISON OF THE ALGORITHMS IN MULTI-DOMAIN FEATURE EXTRACTION OF ERP DATA BASED ON COUPLED NCPD MODEL

Methods	ADMM	ALS	MU	fHALS	APG	Ira&APG	*step-1	*step-2
Fit	0.8222	0.7639	0.8375	0.8350	0.8491	0.8490	0.9901	0.8493
Time	63.392	69.123	54.962	62.978	56.050	12.317	0.9768	11.340
MCC-Mean	0.7143	0.6318	0.7936	0.8567	0.8828	0.8777	-	-
MCC-SD	0.1471	0.1681	0.1155	0.1118	0.0796	0.0799	-	-

decomposition results of ERP data. Figure 5 gives an example illustration of multi-domain features and their corresponding components extracted by CoNCPD-APG algorithm in the 1st run. For multi-domain feature shown in the figure, statistical analysis using t-test reveals the significant difference between RD and AD groups with $t_{20} = 2.0899$, $p = 0.0108$. The relevant temporal component (latency peaks around 150 ms) and spectral component (spectrum peaks around 5 Hz) closely match the property of mismatch negativity component [56]. The corresponding topography denotes that the difference of RD and AD groups may appear in the central and left hemisphere [56].

We adopt three steps to verify the stability of multi-domain feature extraction of all the compared algorithms in 100 runs. (1) We select the multi-domain features and their parallel three components in the 1st runs of 5 algorithms. (2) We average the selected ones separately as a set of template patterns, which are termed as \mathbf{u}_{temp}^{fea} , \mathbf{u}_{temp}^{tem} , \mathbf{u}_{temp}^{spe} and \mathbf{u}_{temp}^{spa} . (3) We define the maximum correlation coefficient (MCC) between template patterns and feature-based components of k th runs as follows

$$MCC(k) = \max [\text{corr}(\mathbf{u}_{temp}^{fea}, \mathbf{U}_k^{fea}) \otimes \text{corr}(\mathbf{u}_{temp}^{tem}, \mathbf{U}_k^{tem}) \otimes \text{corr}(\mathbf{u}_{temp}^{spe}, \mathbf{U}_k^{spe}) \otimes \text{corr}(\mathbf{u}_{temp}^{spa}, \mathbf{U}_k^{spa})] \quad (24)$$

where k denotes the run number and corr is a matlab function which returns a vector containing the pairwise linear correlation coefficient between \mathbf{u} and \mathbf{U} . \mathbf{U}_k^{fea} , \mathbf{U}_k^{tem} , \mathbf{U}_k^{spe} and \mathbf{U}_k^{spa} represent multi-domain features and their corresponding temporal, spectral and spatial components in the k th run, respectively. Obviously, if the MCC is close to 1, it means that the extraction of multi-domain features is more stable.

Table V gives the average tensor fit and running time from 100 independent runs for ERP data, as well as the means and SDs of MCCs for multi-domain features. We can see that the proposed CoNCPD-APG and IraCoNCPD-APG algorithms are superior to competitors in terms of decomposition accuracy and multi-domain feature extraction stability. Interestingly, although some algorithms achieve good performance in data fittings, their multi-domain feature extraction is less stable. This experiment also demonstrates the positive effect of low-rank approximation in large-scale tensor coupling analysis, we can see that the first step of the algorithm takes very little time, but saves a lot of time for the second step.

D. Real-world Ongoing EEG data

In this part, we apply the proposed algorithms to the joint analysis of ongoing EEG data, which are collected from 14 participants when listening to an 8.5-min piece of

⁴http://www.escience.cn/people/cong/AdvancedSP_ERP.html



Fig. 4. Illustration of original (1st row), noisy (2nd row), and recovered (3rd row) face images, as well as common (4th and 5th rows) and individual (6th row) face image features obtained by CoNCPD-APG algorithm for image reconstruction and denoising with 0.1 salt-and-pepper noise

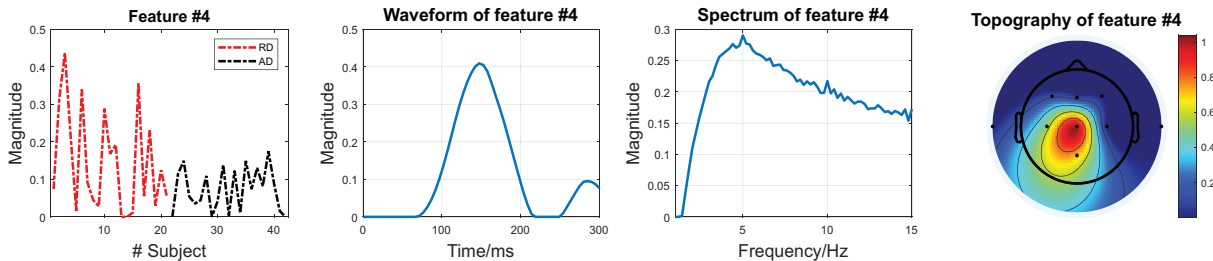


Fig. 5. An example of multi-domain feature and its related temporal, spectral and spatial components of ERP data extracted by CoNCPD-APG algorithm

modern tango. After the short-time Fourier transform and necessary preprocessing, we eventually generate 14 third-order tensors with the size of 46 (frequency bins) \times 510 (time samples) \times 64 (space channels) for 14 participants. Detailed information about data acquisition and preprocessing can be found in [11, 57]. For ease of comparison, following [11], which assumes that coupling information exists in both spatial and spectral modes, we set the number of components as the number of components were respectively selected as {44, 34, 36, 38, 36, 39, 35, 35, 34, 37, 33, 36, 34, 35}, and set the number of component components as $L_{1,2,3} = [26, 26, 0]$. Next, we follow the flowchart of ongoing EEG data processing and analysis proposed in [11], including data acquisition & preprocessing, musical feature extraction, tensor representation, algorithm implementation, correlation analysis, hierarchical clustering, and cluster selection of interest.

Finally, we conclude three clusters of interest, where the topographies reveal activations in centro-parietal, occipito-parietal, and frontal regions, as well as oscillations mainly

in theta, alpha, and theta-alpha frequency bands, see Fig. 6, and these findings are consistent with the previous study [11]. Moreover, the CoNCPD-APG algorithm shows more stable performance in extracting clusters of interest, as the probability of clusters #I, #II, and #III appearing in 100 runs reaches 85%, 99%, and 93%, while the probability of clusters #I, #II, and #III obtained by the IraCoNCPD-APG algorithm is 75%, 94%, and 89%, respectively. Meanwhile, the average inter-run correlations of clusters #I, #II, and #III of the CoNCPD-APG algorithm reached 0.9625, 0.9903, and 0.945. Although the performance of the IraCoNCPD-APG algorithm declined, it also reached 0.9573, 0.9859, and 0.9521, respectively. In addition, in terms of convergence, the CoNCPD-APG algorithm performs slightly better than the IraCoNCPD-APG algorithm in tensor fitting (0.7219 vs 0.7143), but requires more running time (49.27s vs 7.86s).

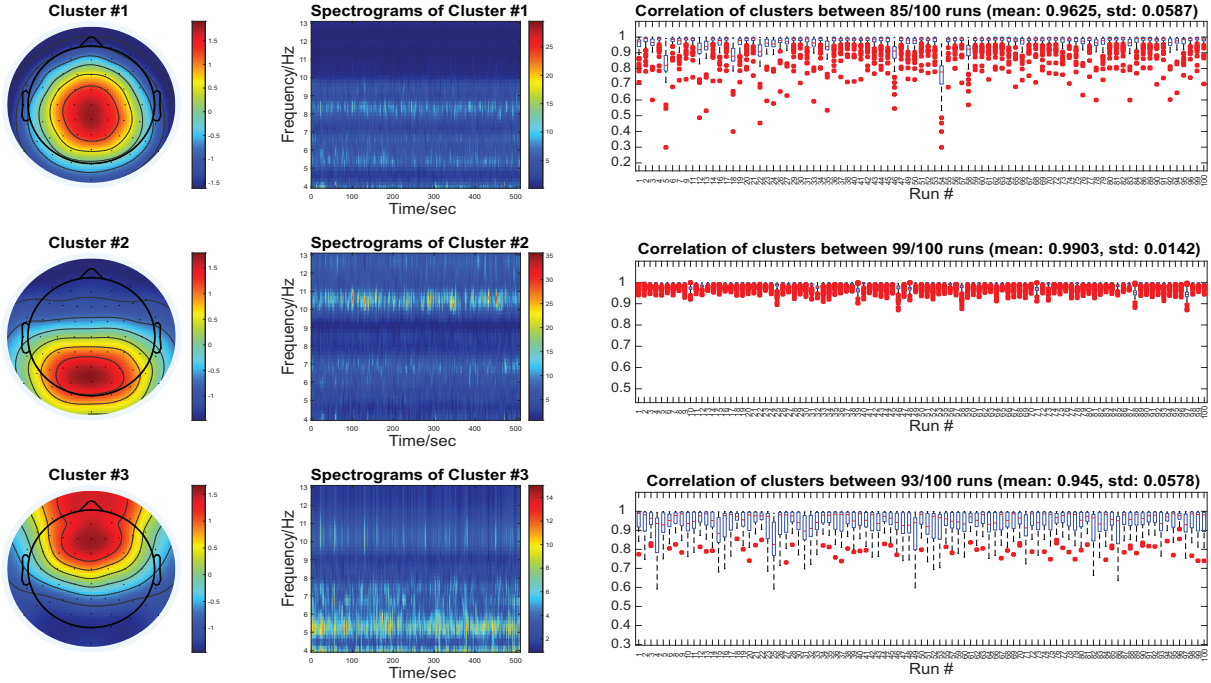


Fig. 6. Illustrations (Topography, spectrogram, and correlation) of clusters #I, #II and #III obtained from 100 runs by the CoNCPD-APG algorithm

V. CONCLUSION

In this study, we addressed the problem of coupled tensor decomposition, focusing on the simultaneous decomposition of nonnegative multi-block tensors. To enhance convergence speed and optimization accuracy, we first proposed a coupled nonnegative CANDECOMP/PARAFAC decomposition algorithm based on the alternating proximal gradient (APG) method, referred to as CoNCPD-APG. Building on this, we further proposed the IraCoNCPD-APG algorithm combining APG and low-rank approximation. We also gave some discussions on the properties of these algorithms as well as some implementation remarks. Experiments of synthetic data, real-world face image data, and event-related potential (ERP) data were conducted to compare the proposed algorithms with fast hierarchical alternating least squares (fHALS), multiplicative updating (MU), and alternating least squares (ALS)-based algorithms in the context of coupled NCPD problems. Results illustrated that our proposed algorithms are superior to competitors in terms of decomposition accuracy, image reconstruction capability, and multi-domain feature extraction stability, and also demonstrated that the introduction of low-rank approximation can greatly improve the computation efficiency without compromising the decomposition quality.

Determining the number of coupled components depends on the validity of potential assumptions and relevant prior knowledge. So far, its selection in real-world applications remains somewhat subjective, making it an open issue and a subject for our future research. Furthermore, exploring linearly soft coupling will also be a focus of our future work.

ACKNOWLEDGMENT

This work is supported by National Natural Science Foundation of China (Grant No.91748105), National Foundation

in China (No. JCKY2019110B009 & 2020-JCJQ-JJ-252), the Fundamental Research Funds for the Central Universities [DUT20LAB303& DUT20LAB308] in Dalian University of Technology in China, Dalian Science and Technology Talent Innovation Support Project (No.2023RY034), and Dalian life and health guidance program project (No.2024033). This study is to memorize Prof. Tapani Ristaniemi for his great help to the authors, Fengyu Cong and Xiulin Wang.

APPENDIX A

ALGORITHM DERIVATIONS AND PARAMETER SETTINGS

For completeness of this paper, in this section, some steps of algorithm derivations and relevant parameter settings will be further explained below.

1) **CoNCPD-APG algorithm:** Following [43, 44], by using Lagrange multiplier method, we obtain (9), (12), (14) and (15) from (8) and (11). When updating the core tensor $\mathcal{D}^{(s)}$, by keeping all factor matrices $\mathcal{U}^{(n,s)}$ fixed, we first convert (7) to

$$F_d = \frac{1}{2} \left\| \text{vec}(\mathcal{M}^{(s)}) - \mathcal{U}^{(s)\odot} \text{ddiag}(\mathcal{D}^{(s)}) \right\|_F^2 \quad (25)$$

where $\text{vec}(\mathcal{M}^{(s)})$ denotes the vectorization of tensor $\mathcal{M}^{(s)}$. Mathematically, the squared Frobenius norm of a matrix can be replaced by the trace of multiplication of the matrix and its transpose. Then (25) can be represented as:

$$F_d = \frac{1}{2} \text{tr} \left[\left(\text{vec}(\mathcal{M}^{(s)}) - \mathcal{U}^{(s)\odot} \text{ddiag}(\mathcal{D}^{(s)}) \right)^T \left(\text{vec}(\mathcal{M}^{(s)}) - \mathcal{U}^{(s)\odot} \text{ddiag}(\mathcal{D}^{(s)}) \right) \right] \quad (26)$$

According to trace property, the block-partial gradient $\hat{\mathcal{G}}^{(s)}$ of (26) with respect to $\hat{\mathcal{D}}^{(s)}$ can be calculated by

$$\begin{aligned}\hat{\mathcal{G}}^{(s)} &= \nabla_{\hat{\mathcal{D}}^{(s)}} F_d \\ &= \text{ddiag} \left[\left(\mathbf{U}^{(s)\odot} \right)^T \mathbf{U}^{(s)\odot} \text{ddiag} \left(\hat{\mathcal{D}}^{(s)} \right) \right] \\ &\quad - \text{ddiag} \left[\left(\mathbf{U}^{(s)\odot} \right)^T \text{vec} \left(\mathcal{M}^{(s)} \right) \right]\end{aligned}\quad (27)$$

where the outer notation ‘ddiag’ means the tensorization from a vector to a super-diagonal tensor, which is the reverse operation of inner one. Using the property of Khatri-Rao product, we can efficiently calculate $(\mathbf{U}^{(s)\odot})^T \mathbf{U}^{(s)\odot}$ by

$$\left(\mathbf{U}^{(s)\odot} \right)^T \mathbf{U}^{(s)\odot} = \left(\mathbf{U}^{(s)T} \mathbf{U}^{(s)} \right)^{\otimes} \quad (28)$$

When updating the factor matrix (without coupling information) $\mathbf{U}^{(n,s)}$, by keeping all other variables $\mathbf{U}^{(m,s)}$, $m \neq n$ and $\mathcal{D}^{(s)}$ fixed, (7) is represented as follows:

$$F_u = \frac{1}{2} \left\| \mathcal{M}_{(n)}^{(s)} - \mathbf{U}^{(n,s)} \mathbf{D}^{(s)} \left(\mathbf{U}^{(s)\odot-n} \right)^T \right\|_F^2 \quad (29)$$

where $\mathcal{M}_{(n)}^{(s)}$ denotes the mode- n matricization of $\mathcal{M}^{(s)}$. $\mathbf{D}^{(s)}$ is a diagonal matrix and its diagonal elements correspond to the super-diagonal elements of core tensor $\mathcal{D}^{(s)}$. Similarly, the block-partial gradient $\hat{\mathcal{G}}^{(n,s)}$ of (29) at $\hat{\mathbf{U}}^{(n,s)}$ can be calculated as:

$$\begin{aligned}\hat{\mathcal{G}}^{(n,s)} &= \nabla_{\hat{\mathbf{U}}^{(n,s)}} F_u \\ &= \hat{\mathbf{U}}^{(n,s)} \mathbf{D}^{(s)} \left(\mathbf{U}^{(s)\odot-n} \right)^T \mathbf{U}^{(s)\odot-n} \left(\mathbf{D}^{(s)} \right)^T \\ &\quad - \mathcal{M}_{(n)}^{(s)} \mathbf{U}^{(s)\odot-n} \left(\mathbf{D}^{(s)} \right)^T \\ &= \hat{\mathbf{U}}^{(n,s)} \mathbf{D}^{(s)} \left(\mathbf{U}^{(s)T} \mathbf{U}^{(s)} \right)^{\otimes-n} \mathbf{D}^{(s)} \\ &\quad - \mathcal{M}_{(n)}^{(s)} \mathbf{U}^{(s)\odot-n} \mathbf{D}^{(s)}\end{aligned}\quad (30)$$

However, when updating the factor matrix $\mathbf{U}^{(n,s)}$ which consists of two parts: $\mathbf{U}_C^{(n,s)}$ and $\mathbf{U}_I^{(n,s)}$, we first substitute $\mathbf{U}^{(n,s)} = \left[\mathbf{U}_C^{(n,s)} \quad \mathbf{U}_I^{(n,s)} \right]$ into (29) and have

$$F_{ci} = \frac{1}{2} \left\| \mathcal{M}_{(n)}^{(s)} - \left[\mathbf{U}_C^{(n,s)} \quad \mathbf{U}_I^{(n,s)} \right] \mathbf{D}^{(s)} \left(\mathbf{U}^{(s)\odot-n} \right)^T \right\|_F^2 \quad (31)$$

Let $\mathbf{B}^{(n,s)} = \mathbf{D}^{(s)} \left(\mathbf{U}^{(s)\odot-n} \right)^T \in \mathbb{R}_+^{R^{(s)} \times \prod_{m \neq n}^N I_m}$. Let $\hat{\mathcal{G}}_C^{(n,s)}$ denote the block-partial gradient of (31) at $\hat{\mathbf{U}}_C^{(n,s)}$, which can be calculated as:

$$\begin{aligned}\hat{\mathcal{G}}_C^{(n,s)} &= \nabla_{\hat{\mathbf{U}}_C^{(n,s)}} F_{ci} \\ &= \hat{\mathbf{U}}_C^{(n,s)} \mathbf{B}_C^{(n,s)} \left(\mathbf{B}_C^{(n,s)} \right)^T \\ &\quad - \left(\mathcal{M}_{(n)}^{(s)} - \hat{\mathbf{U}}_I^{(n,s)} \mathbf{B}_I^{(n,s)} \right) \left(\mathbf{B}_C^{(n,s)} \right)^T \\ &= \left(\hat{\mathbf{U}}_C^{(n,s)} \mathbf{B}_C^{(n,s)} - \mathcal{M}_{(n)}^{(s)} \right) \left(\mathbf{B}_C^{(n,s)} \right)^T\end{aligned}\quad (32)$$

where $\hat{\mathbf{U}}_C^{(n,s)}$ denotes an extrapolated point of $\mathbf{U}_C^{(n,s)}$. $\mathbf{B}^{(n,s)} = \left[\mathbf{B}_C^{(n,s)}; \mathbf{B}_I^{(n,s)} \right]$, $\mathbf{B}_C^{(n,s)} \in \mathbb{R}_+^{L_n \times \prod_{m \neq n}^N I_m}$ and

$\mathbf{B}_I^{(n,s)} \in \mathbb{R}_+^{(R^{(s)} - L_n) \times \prod_{m \neq n}^N I_m}$. From (30) and (32), it can be inferred that $\hat{\mathcal{G}}_C^{(n,s)}$ is equal to $\hat{\mathcal{G}}_{:,1:L_n}^{(n,s)}$. Analogously, the block-partial gradient $\hat{\mathcal{G}}_I^{(n,s)}$ at $\hat{\mathbf{U}}_I^{(n,s)}$ can be obtained as $\hat{\mathcal{G}}_{:,L_n:R^{(s)}}^{(n,s)}$ and $\hat{\mathcal{G}}^{(n,s)} = \left[\hat{\mathcal{G}}_C^{(n,s)} \quad \hat{\mathcal{G}}_I^{(n,s)} \right]$.

2) **Parameter settings:** Consider updating $\mathcal{D}^{(s)}$ and $\mathbf{U}^{(n,s)}$ at the k th iteration. Following [-], we set the Lipschitz constants $L_{d,k-1}^{(s)}$ and $L_{u,k-1}^{(n,s)}$ as:

$$L_{d,k-1}^{(s)} = \left\| \left(\mathbf{U}_{k-1}^{(s)\odot} \right)^T \mathbf{U}_{k-1}^{(s)\odot} \right\| \quad (33)$$

and

$$L_{u,k-1}^{(n,s)} = \left\| \mathbf{D}_{k-1}^{(s)} \left(\mathbf{U}_{k-1}^{(s)\odot-n} \right)^T \mathbf{U}_{k-1}^{(s)\odot-n} \mathbf{D}_{k-1}^{(s)} \right\| \quad (34)$$

where $\| \cdot \|$ denotes the spectral norm. Using the property of Khatri-Rao product, we can also efficiently calculate $L_{d,k-1}^{(s)}$ and $L_{u,k-1}^{(n,s)}$ through

$$\begin{aligned}\left(\mathbf{U}_{k-1}^{(s)\odot} \right)^T \mathbf{U}_{k-1}^{(s)\odot} &= \left[\left(\mathbf{U}_{k-1}^{(n,s)} \right)^T \mathbf{U}_{k-1}^{(n,s)} \right]^{\otimes} \\ \left(\mathbf{U}_{k-1}^{(s)\odot-n} \right)^T \mathbf{U}_{k-1}^{(s)\odot-n} &= \left[\left(\mathbf{U}_{k-1}^{(m,s)} \right)^T \mathbf{U}_{k-1}^{(m,s)} \right]^{\otimes-n}\end{aligned}\quad (35)$$

We take the extrapolation weights as

$$w_{d,k-1}^{(s)} = \min \left(\hat{w}_{k-1}, \delta_w \sqrt{\frac{L_{d,k-2}^{(s)}}{L_{d,k-1}^{(s)}}} \right) \quad (36)$$

and

$$w_{u,k-1}^{(n,s)} = \min \left(\hat{w}_{k-1}, \delta_w \sqrt{\frac{L_{u,k-2}^{(n,s)}}{L_{u,k-1}^{(n,s)}}} \right) \quad (37)$$

where $\delta_w < 1$ is predefined (e.g., 0.9999, [45]), and $\hat{w}_{k-1} = \frac{t_{k-1}-1}{t_k}$ with $t_0 = 1$ and $t_k = \frac{1}{2} \left(1 + \sqrt{1 + 4t_{k-1}^2} \right)$. Moreover, we define the extrapolation at points $\mathcal{D}_{k-1}^{(s)}$ and $\mathbf{U}_{k-1}^{(n,s)}$ as

$$\hat{\mathcal{D}}_{k-1}^{(s)} = \mathcal{D}_{k-1}^{(s)} + w_{d,k-1}^{(s)} \left(\mathcal{D}_{k-1}^{(s)} - \mathcal{D}_{k-2}^{(s)} \right) \quad (38)$$

and

$$\hat{\mathbf{U}}_{k-1}^{(n,s)} = \mathbf{U}_{k-1}^{(n,s)} + w_{u,k-1}^{(n,s)} \left(\mathbf{U}_{k-1}^{(n,s)} - \mathbf{U}_{k-2}^{(n,s)} \right) \quad (39)$$

APPENDIX B PROOF OF PROPOSITION 1

(i) Let $\zeta(\mathcal{X}^{(s)}, \mathbf{U}^{(n,s)})|_{\mathbf{U}^{(n,s)} \geq 0, \mathcal{X}^{(s)} \in \mathbb{R}^{I_1 \times I_2 \times \dots \times I_N}} = \sum_{s=1}^S \left[\left\| \mathcal{Y}^{(s)} - \mathcal{X}^{(s)} \right\|_F + \left\| \mathcal{X}^{(s)} - \left[\mathbf{U}^{(1,s)}, \mathbf{U}^{(2,s)}, \dots, \mathbf{U}^{(N,s)} \right] \right\|_F \right]$.

Therefore, for $\forall \mathbf{U}^{(n,s)} \geq 0$ and $\mathbf{x}^{(s)} \in \mathbb{R}^{I_1 \times I_2 \times \dots \times I_N}$, we have

$$\begin{aligned} & \sum_{s=1}^S \left[\left\| \mathbf{y}^{(s)} - \mathbf{x}^{(s)} \right\|_F + \left\| \mathbf{x}^{(s)} - \left[\mathbf{U}^{(1,s)}, \mathbf{U}^{(2,s)}, \dots, \mathbf{U}^{(N,s)} \right] \right\|_F \right] \\ & \geq \sum_{s=1}^S \left[\left\| \mathbf{y}^{(s)} - \left[\mathbf{U}^{(1,s)}, \mathbf{U}^{(2,s)}, \dots, \mathbf{U}^{(N,s)} \right] \right\|_F \right] \\ & \geq \sum_{s=1}^S \left[\left\| \mathbf{y}^{(s)} - \left[\mathbf{U}_{\diamond}^{(1,s)}, \mathbf{U}_{\diamond}^{(2,s)}, \dots, \mathbf{U}_{\diamond}^{(N,s)} \right] \right\|_F \right] \\ & = \sum_{s=1}^S \epsilon_{(s)}^{\diamond} \end{aligned} \quad (40)$$

Obviously, ζ can reach the lower bound if $\mathbf{U}^{(n,s)} = \mathbf{U}_{\diamond}^{(n,s)}$ and $\mathbf{x}^{(s)} = \left[\mathbf{U}_{\diamond}^{(1,s)}, \mathbf{U}_{\diamond}^{(2,s)}, \dots, \mathbf{U}_{\diamond}^{(N,s)} \right]$. This completes the proof of (i).

(ii) According to the definition of $\epsilon_{(s)}^{\diamond}$, first we can have

$$\sum_{s=1}^S \epsilon_{(s)}^{\diamond} \leq \sum_{s=1}^S \left\| \mathbf{y}^{(s)} - \left[\vec{\mathbf{U}}^{(1,s)}, \vec{\mathbf{U}}^{(2,s)}, \dots, \vec{\mathbf{U}}^{(N,s)} \right] \right\|_F \quad (41)$$

Then we have

$$\begin{aligned} & \sum_{s=1}^S \left\| \mathbf{y}^{(s)} - \left[\vec{\mathbf{U}}^{(1,s)}, \vec{\mathbf{U}}^{(2,s)}, \dots, \vec{\mathbf{U}}^{(N,s)} \right] \right\|_F \\ & \leq \sum_{s=1}^S \left[\left\| \mathbf{y}^{(s)} - \mathbf{x}^{(s)} \right\|_F + \left\| \mathbf{x}^{(s)} - \left[\vec{\mathbf{U}}^{(1,s)}, \vec{\mathbf{U}}^{(2,s)}, \dots, \vec{\mathbf{U}}^{(N,s)} \right] \right\|_F \right] \\ & = \sum_{s=1}^S \left[\theta^{(s)} + \left\| \mathbf{x}^{(s)} - \left[\vec{\mathbf{U}}^{(1,s)}, \vec{\mathbf{U}}^{(2,s)}, \dots, \vec{\mathbf{U}}^{(N,s)} \right] \right\|_F \right] \\ & \leq \sum_{s=1}^S \left[\theta^{(s)} + \left\| \mathbf{x}^{(s)} - \left[\mathbf{U}_{\diamond}^{(1,s)}, \mathbf{U}_{\diamond}^{(2,s)}, \dots, \mathbf{U}_{\diamond}^{(N,s)} \right] \right\|_F \right] \\ & \leq \sum_{s=1}^S \left[\theta^{(s)} + \left\| \mathbf{x}^{(s)} - \mathbf{y}^{(s)} \right\|_F + \left\| \mathbf{y}^{(s)} - \left[\mathbf{U}_{\diamond}^{(1,s)}, \mathbf{U}_{\diamond}^{(2,s)}, \dots, \mathbf{U}_{\diamond}^{(N,s)} \right] \right\|_F \right] \\ & \leq \sum_{s=1}^S \left[2\theta^{(s)} + \epsilon_{(s)}^{\diamond} \right] \end{aligned} \quad (42)$$

This completes the proof of (ii).

REFERENCES

[1] F. L. Hitchcock, “The expression of a tensor or a polyadic as a sum of products,” *Journal of Mathematics and Physics*, vol. 6, no. 1-4, pp. 164–189, 1927.

[2] R. A. Harshman *et al.*, “Foundations of the parafac procedure: Models and conditions for an” explanatory” multimodal factor analysis,” 1970.

[3] J. D. Carroll and J.-J. Chang, “Analysis of individual differences in multidimensional scaling via an n-way generalization of “eckart-young” decomposition,” *Psychometrika*, vol. 35, no. 3, pp. 283–319, 1970.

[4] A. Cichocki, R. Zdunek, A. H. Phan, and S.-i. Amari, *Nonnegative matrix and tensor factorizations: applications to exploratory multi-way data analysis and blind source separation*. John Wiley & Sons, 2009.

[5] F. Cong, Q.-H. Lin, L.-D. Kuang, X.-F. Gong, P. Astikainen, and T. Ristaniemi, “Tensor decomposition of eeg signals: a brief review,” *Journal of neuroscience methods*, vol. 248, pp. 59–69, 2015.

[6] F. Cong, A.-H. Phan, P. Astikainen, Q. Zhao, Q. Wu, J. K. Hietanen, T. Ristaniemi, and A. Cichocki, “Multi-domain feature extraction for small event-related potentials through nonnegative multi-way array decomposition from low dense array eeg,” *International journal of neural systems*, vol. 23, no. 02, p. 1350006, 2013.

[7] T. G. Kolda and B. W. Bader, “Tensor decompositions and applications,” *SIAM review*, vol. 51, no. 3, pp. 455–500, 2009.

[8] A. Cichocki, D. Mandic, L. De Lathauwer, G. Zhou, Q. Zhao, C. Caiafa, and H. A. Phan, “Tensor decompositions for signal processing applications: From two-way to multiway component analysis,” *IEEE signal processing magazine*, vol. 32, no. 2, pp. 145–163, 2015.

[9] N. D. Sidiropoulos, L. De Lathauwer, X. Fu, K. Huang, E. E. Papalexakis, and C. Faloutsos, “Tensor decomposition for signal processing and machine learning,” *IEEE Transactions on Signal Processing*, vol. 65, no. 13, pp. 3551–3582, 2017.

[10] G. Zhou, Q. Zhao, Y. Zhang, T. Adali, S. Xie, and A. Cichocki, “Linked component analysis from matrices to high-order tensors: Applications to biomedical data,” *Proceedings of the IEEE*, vol. 104, no. 2, pp. 310–331, 2016.

[11] X. Wang, W. Liu, P. Toivainen, T. Ristaniemi, and F. Cong, “Group analysis of ongoing eeg data based on fast double-coupled nonnegative tensor decomposition,” *Journal of neuroscience methods*, vol. 330, p. 108502, 2020.

[12] Y. Jonmohamadi, S. Muthukumaraswamy, J. Chen, J. Roberts, R. Crawford, and A. Pandey, “Extraction of common task features in eeg-fMRI data using coupled tensor-tensor decomposition,” *bioRxiv*, p. 685941, 2019.

[13] X. Gong, Q. Lin, F. Cong, and L. De Lathauwer, “Double coupled canonical polyadic decomposition for joint blind source separation,” *IEEE Transactions on Signal Processing*, vol. 66, no. 13, pp. 3475–3490, 2018.

[14] M. Sørensen, I. Domanov, and L. De Lathauwer, “Coupled canonical polyadic decompositions and (coupled) decompositions in multilinear rank- $(l_r, n, l_r, n, 1)$ terms—part ii: Algorithms,” *SIAM Journal on Matrix Analysis and Applications*, vol. 36, no. 3, pp. 1015–1045, 2015.

[15] B. Hunyadi, P. Dupont, W. Van Paesschen, and S. Van Huffel, “Tensor decompositions and data fusion in epileptic electroencephalography and functional magnetic resonance imaging data,” *Wiley Interdisciplinary Reviews: Data Mining and Knowledge Discovery*, vol. 7, no. 1, p. e1197, 2017.

[16] Z. Xue, S. Yang, H. Zhang, and P. Du, “Coupled higher-order tensor factorization for hyperspectral and lidar data fusion and classification,” *Remote Sensing*, vol. 11, no. 17, p. 1959, 2019.

- [17] A. Cichocki, “Tensor decompositions: a new concept in brain data analysis?” *arXiv preprint arXiv:1305.0395*, 2013.
- [18] V. D. Calhoun, J. Liu, and T. Adalı, “A review of group ica for fmri data and ica for joint inference of imaging, genetic, and erp data,” *Neuroimage*, vol. 45, no. 1, pp. S163–S172, 2009.
- [19] X.-F. Gong, X.-L. Wang, and Q.-H. Lin, “Generalized non-orthogonal joint diagonalization with lu decomposition and successive rotations,” *IEEE Transactions on Signal Processing*, vol. 63, no. 5, pp. 1322–1334, 2015.
- [20] M. Mørup, “Applications of tensor (multiway array) factorizations and decompositions in data mining,” *Wiley Interdisciplinary Reviews: Data Mining and Knowledge Discovery*, vol. 1, no. 1, pp. 24–40, 2011.
- [21] T. Yokota, A. Cichocki, and Y. Yamashita, “Linked parafac/cp tensor decomposition and its fast implementation for multi-block tensor analysis,” in *International Conference on Neural Information Processing*. Springer, 2012, pp. 84–91.
- [22] X. Wang, C. Zhang, T. Ristaniemi, and F. Cong, “Generalization of linked canonical polyadic tensor decomposition for group analysis,” in *International Symposium on Neural Networks*. Springer, 2019, pp. 180–189.
- [23] G. Zhou, A. Cichocki, Y. Zhang, and D. P. Mandic, “Group component analysis for multiblock data: Common and individual feature extraction,” *IEEE transactions on neural networks and learning systems*, vol. 27, no. 11, pp. 2426–2439, 2015.
- [24] E. Acar, T. G. Kolda, and D. M. Dunlavy, “All-at-once optimization for coupled matrix and tensor factorizations,” *arXiv preprint arXiv:1105.3422*, 2011.
- [25] E. Acar, Y. Levin-Schwartz, V. D. Calhoun, and T. Adalı, “Acmtf for fusion of multi-modal neuroimaging data and identification of biomarkers,” in *2017 25th European Signal Processing Conference (EUSIPCO)*. IEEE, 2017, pp. 643–647.
- [26] C. Chatzichristos, M. Davies, J. Escudero, E. Kofidis, and S. Theodoridis, “Fusion of eeg and fmri via soft coupled tensor decompositions,” in *2018 26th European Signal Processing Conference (EUSIPCO)*. IEEE, 2018, pp. 56–60.
- [27] C. Schenker, X. Wang, and E. Acar, “Parafac2-based coupled matrix and tensor factorizations,” in *ICASSP 2023-2023 IEEE International Conference on Acoustics, Speech and Signal Processing (ICASSP)*. IEEE, 2023, pp. 1–5.
- [28] X. Wang, W. Liu, X. Wang, Z. Mu, J. Xu, Y. Chang, Q. Zhang, J. Wu, and F. Cong, “Shared and unshared feature extraction in major depression during music listening using constrained tensor factorization,” *Frontiers in Human Neuroscience*, vol. 15, p. 799288, 2021.
- [29] R. Zdunek, K. Fonał, and A. Wołczowski, “Linked cp tensor decomposition algorithms for shared and individual feature extraction,” *Signal Processing: Image Communication*, vol. 73, pp. 37–52, 2019.
- [30] C. I. Kanatsoulis, X. Fu, N. D. Sidiropoulos, and W.-K. Ma, “Hyperspectral super-resolution: A coupled tensor factorization approach,” *IEEE Transactions on Signal Processing*, vol. 66, no. 24, pp. 6503–6517, 2018.
- [31] S. Li, R. Dian, L. Fang, and J. M. Bioucas-Dias, “Fusing hyperspectral and multispectral images via coupled sparse tensor factorization,” *IEEE Transactions on Image Processing*, vol. 27, no. 8, pp. 4118–4130, 2018.
- [32] T. Xu, T.-Z. Huang, L.-J. Deng, J.-L. Xiao, C. Broni-Bediako, J. Xia, and N. Yokoya, “A coupled tensor double-factor method for hyperspectral and multispectral image fusion,” *IEEE Transactions on Geoscience and Remote Sensing*, 2024.
- [33] M. Sørensen and L. De Lathauwer, “Coupled tensor decompositions for applications in array signal processing,” in *2013 5th IEEE International Workshop on Computational Advances in Multi-Sensor Adaptive Processing (CAMSAP)*. IEEE, 2013, pp. 228–231.
- [34] —, “Multidimensional harmonic retrieval via coupled canonical polyadic decomposition—part i: Model and identifiability,” *IEEE Transactions on Signal Processing*, vol. 65, no. 2, pp. 517–527, 2016.
- [35] —, “Multidimensional harmonic retrieval via coupled canonical polyadic decomposition—part ii: Algorithm and multirate sampling,” *IEEE Transactions on Signal Processing*, vol. 65, no. 2, pp. 528–539, 2016.
- [36] B. Ermiş, E. Acar, and A. T. Cemgil, “Link prediction in heterogeneous data via generalized coupled tensor factorization,” *Data Mining and Knowledge Discovery*, vol. 29, no. 1, pp. 203–236, 2015.
- [37] E. Acar, R. Bro, and A. K. Smilde, “Data fusion in metabolomics using coupled matrix and tensor factorizations,” *Proceedings of the IEEE*, vol. 103, no. 9, pp. 1602–1620, 2015.
- [38] G. Zhou, A. Cichocki, and S. Xie, “Fast nonnegative matrix/tensor factorization based on low-rank approximation,” *IEEE Transactions on Signal Processing*, vol. 60, no. 6, pp. 2928–2940, 2012.
- [39] Y. Zhang, G. Zhou, Q. Zhao, A. Cichocki, and X. Wang, “Fast nonnegative tensor factorization based on accelerated proximal gradient and low-rank approximation,” *Neurocomputing*, vol. 198, pp. 148–154, 2016.
- [40] N. Parikh, S. Boyd *et al.*, “Proximal algorithms,” *Foundations and Trends® in Optimization*, vol. 1, no. 3, pp. 127–239, 2014.
- [41] Y. E. Nesterov, “A method for solving the convex programming problem with convergence rate $o(1/k^2)$,” in *Dokl. akad. nauk Ssr*, vol. 269, 1983, pp. 543–547.
- [42] A. Beck and M. Teboulle, “A fast iterative shrinkage-thresholding algorithm for linear inverse problems,” *SIAM journal on imaging sciences*, vol. 2, no. 1, pp. 183–202, 2009.
- [43] N. Guan, D. Tao, Z. Luo, and B. Yuan, “Nenmf: An optimal gradient method for nonnegative matrix factorization,” *IEEE Transactions on Signal Processing*, vol. 60, no. 6, pp. 2882–2898, 2012.
- [44] Y. Xu and W. Yin, “A block coordinate descent method for regularized multiconvex optimization with applications to nonnegative tensor factorization and completion,” *SIAM Journal on imaging sciences*, vol. 6, no. 3, pp.

- 1758–1789, 2013.
- [45] Y. Xu, “Alternating proximal gradient method for sparse nonnegative tucker decomposition,” *Mathematical Programming Computation*, vol. 7, no. 1, pp. 39–70, 2015.
- [46] F. Cong, G. Zhou, P. Astikainen, Q. Zhao, Q. Wu, A. K. Nandi, J. K. Hietanen, T. Ristaniemi, and A. Cichocki, “Low-rank approximation based non-negative multi-way array decomposition on event-related potentials,” *International journal of neural systems*, vol. 24, no. 08, p. 1440005, 2014.
- [47] C. Schenker, J. E. Cohen, and E. Acar, “A flexible optimization framework for regularized matrix-tensor factorizations with linear couplings,” *IEEE Journal of Selected Topics in Signal Processing*, vol. 15, no. 3, pp. 506–521, 2020.
- [48] G. Hu, H. Li, W. Zhao, Y. Hao, Z. Bai, L. D. Nickerson, and F. Cong, “Discovering hidden brain network responses to naturalistic stimuli via tensor component analysis of multi-subject fmri data,” *NeuroImage*, vol. 255, p. 119193, 2022.
- [49] X. Wang, T. Ristaniemi, and F. Cong, “Fast implementation of double-coupled nonnegative canonical polyadic decomposition,” in *ICASSP 2019-2019 IEEE International Conference on Acoustics, Speech and Signal Processing (ICASSP)*. IEEE, 2019, pp. 8588–8592.
- [50] A. Cichocki and A.-H. Phan, “Fast local algorithms for large scale nonnegative matrix and tensor factorizations,” *IEICE transactions on fundamentals of electronics, communications and computer sciences*, vol. 92, no. 3, pp. 708–721, 2009.
- [51] D. D. Lee and H. S. Seung, “Learning the parts of objects by non-negative matrix factorization,” *Nature*, vol. 401, no. 6755, p. 788, 1999.
- [52] H. Lee and S. Choi, “Group nonnegative matrix factorization for EEG classification,” in *Artificial Intelligence and Statistics*, 2009, pp. 320–327.
- [53] S. Boyd, N. Parikh, E. Chu, B. Peleato, J. Eckstein *et al.*, “Distributed optimization and statistical learning via the alternating direction method of multipliers,” *Foundations and Trends® in Machine Learning*, vol. 3, no. 1, pp. 1–122, 2011.
- [54] A. S. Georghiades, P. N. Belhumeur, and D. J. Kriegman, “From few to many: Illumination cone models for face recognition under variable lighting and pose,” *IEEE transactions on pattern analysis and machine intelligence*, vol. 23, no. 6, pp. 643–660, 2001.
- [55] D. Cai, X. He, and J. Han, “Spectral regression for efficient regularized subspace learning,” in *2007 IEEE 11th international conference on computer vision*. IEEE, 2007, pp. 1–8.
- [56] F. Cong, A. H. Phan, Q. Zhao, T. Huttunen-Scott, J. Kaartinen, T. Ristaniemi, H. Lyytinen, and A. Cichocki, “Benefits of multi-domain feature of mismatch negativity extracted by non-negative tensor factorization from eeg collected by low-density array,” *International journal of neural systems*, vol. 22, no. 06, p. 1250025, 2012.
- [57] F. Cong, V. Alluri, A. K. Nandi, P. Toiviainen, R. Fa, B. Abu-Jamous, L. Gong, B. G. Craenen, H. Poikonen, M. Huottilainen *et al.*, “Linking brain responses to naturalistic music through analysis of ongoing eeg and stimulus features,” *IEEE Transactions on Multimedia*, vol. 15, no. 5, pp. 1060–1069, 2013.